

1 **Combined water table and temperature dynamics control CO₂
2 emission estimates from drained peatlands under rewetting and
3 climate change scenarios**

4 Tanja Denager¹, Jesper Riis Christiansen², Raphael Johannes Maria Schneider¹, Peter Langen³,
5 Thea Quistgaard³, Simon Stisen¹

6 ¹ Department of Hydrology, Geological Survey of Denmark and Greenland, Copenhagen, Denmark

7 ² Forest and Landscape Ecology, Department of Geoscience and Nature Management, Copenhagen University,
8 Denmark

9 ³ Department of Environmental Science, Atmospheric Emissions & Modelling, Aarhus University, Roskilde,
10 Denmark

11 *Correspondence to:* Tanja Denager (tad@geus.dk)

12

13 **Abstract:**

14 This study integrates process-based hydrological modeling and empirical CO₂ flux modeling at a daily
15 temporal resolution to evaluate how peatland hydrology influence CO₂ emissions under scenarios of
16 rewetting and climate change.

17 Following the calibration of a three-dimensional transient groundwater flow model for a peat-
18 dominated catchment, daily groundwater table dynamics were simulated to represent hydrological
19 conditions in drained peat soils. These simulations were coupled with an empirical CO₂ flux model,
20 developed from a comprehensive daily dataset of groundwater table depth, temperature, and soil CO₂
21 flux measurements. The empirical CO₂ flux model captures a clear temperature-dependent response of
22 soil CO₂ emissions to variations in groundwater table depth.

23 By applying this coupled modeling framework, we quantified CO₂ emissions at daily timescales. The
24 results demonstrate that incorporating both temperature sensitivity and high-resolution temporal
25 variability in water level significantly influences projections of CO₂ fluxes. Especially the co-occurrence
26 of elevated air temperature and low groundwater table significantly influence CO₂ emissions under
27 scenarios of rewetting and climate change. These insights highlight the importance of including
28 changing climate conditions in future peatland management strategies for emission inventories.

29 The study illustrates the value of combining detailed hydrological simulations with emission models. It
30 also emphasizes the need for detailed monitoring of greenhouse gas emissions across multiple sites
31 and the development of robust empirical models that can be generalized and spatially upscaled.

32

33 Introduction

34 Drained peatlands are widely accepted as being net greenhouse gas (GHG) sources and rewetting of
35 peatlands is considered an effective means of overall net GHG emission reduction (Leifeld et al., 2019).
36 The depth of the groundwater table below the surface i.e. the water table depth (WTD) largely
37 controls the annual emissions of carbon dioxide (CO₂) and methane (CH₄) from organic soils, where
38 deeper WTD results in CO₂ emissions and a shallow WTD increases CH₄ emissions (Evans et al., 2021).
39 Despite triggering CH₄ emissions, rewetting of organic soils will still lead to a net long-term reduction
40 of GHG emissions (Günther et al., 2020). However, current estimates of GHG emissions from drained
41 and rewetted peatlands are still quite uncertain due to a lack of long-term monitoring and simplified
42 modeling approaches.

43 Commonly adopted methodologies for estimating contribution of organic soils in national GHG
44 inventories (Arents et al., 2018; Evans et al., 2021; Koch et al., 2023; Tiemeyer et al., 2020) are based
45 on empirical response functions between long-term annual mean WTD estimates from data-driven
46 machine learning (ML) models (Bechtold et al., 2014; Koch et al., 2023) and observed net ecosystem
47 GHG budgets (Tiemeyer et al. 2020). Those methodologies allow regional upscaling and integration
48 into national emission estimates.

49 However, significant variability in the observed net ecosystem carbon balance (NECB) used to derive
50 the empirical relationship can be attributed to site-specific factors, including intra-annual (seasonal)
51 WTD and temperature dynamics (Tiemeyer et al., 2020) caused by fluctuating climate. The current
52 GHG inventory methods are not suited to account for extremes such as drought and flooding that have
53 a profound, but temporally limited (days, weeks or months) impact on WTD. Especially the frequency
54 and severity of droughts can have major impacts on the CO₂ emissions as WTD increases together with
55 temperature (Olefeldt et al., 2017). Therefore, temperature changes also directly impact GHG
56 emissions, as soil CO₂ and CH₄ production are temperature sensitive. Currently, the impact of short-
57 term compound events (e.g., simultaneous warm and dry conditions on annual CO₂ emissions from
58 peat soil is little known (Zscheischler et al., 2020) on annual CO₂ emissions from peat soil is little
59 known). Such events can lead to consequences like a deep groundwater table, highlighting the need for
60 improved understanding of how climate variability and long-term change (Olefeldt et al., 2017) affect
61 future CO₂ emissions from both drained and rewetted peatlands.

62 For Denmark, it is generally expected that, as a result of climatic changes, annual mean WTD will
63 decrease (water tables closer to surface). However, this decrease in annual mean WTD is primarily
64 attributed to a decrease in WTD during the wetter winter months, while warmer future summers are
65 anticipated to experience minimal decrease or even increase in summer WTD (water tables deeper
66 below the surface) and more prolonged periods with increased WTD (Henriksen et al., 2023;
67 Seidenfaden et al., 2022).

68 The ML and statistical models of annual mean WTD (Bechtold et al., 2014; Koch et al., 2023) utilized in
69 current national GHG inventories (Gyldenkærne et al., 2025; Koch et al., 2023; Nielsen et al., 2025b;
70 Tiemeyer et al., 2020) effectively reflect the spatial variability at the national scale, but most current
71 ML WTD models are temporally invariant and account for neither inter-annual (between-year)
72 variability nor seasonal or intra-annual variability in WTD or temperature. . To establish WTD-CO₂
73 relations at intra-annual time scales, capable of capturing the impact of short-lived extreme events
74 such as droughts and inundations, WTD time series at these finer temporal resolutions are required.
75 For this, process-based transient 3D hydrological models capable of integrating unsaturated-saturated
76 flow models to predict spatial and temporal variability of WTD are highly useful. Combined with the
77 WTD-CO₂ relation we claim these model outputs can be used to calculate the CO₂ emissions on daily,
78 seasonal, and inter-annual timescales.

79 Such hydrological models provide the potential for improving our estimation of peatland hydrology
80 and thereby the spatio-temporal WTD variability. Improved representation of temporal variability of
81 WTD are needed for refining the current and future GHG estimates that cannot be derived using the
82 simple application of IPCC default emission factors (IPCC, 2014). Process-based hydrological models
83 offer the opportunity to assess the effect of different management strategies and environmental
84 conditions, such as rewetting and climate change.

85 Process-based hydrological models are increasingly being applied to study dynamics of peatland
86 hydrology (Mozafari et al., 2023). For instance, Land Surface Models (LSM) (Bechtold et al., 2019;
87 Largeron et al., 2018; Shi et al., 2015; Yuan et al., 2021) are employed to analyze the soil–plant–
88 atmosphere exchange processes of water, energy and carbon. However, most LSM's rely on a
89 simplified conceptual representation of hydrologic processes and are characterized by coarse spatial
90 scales.

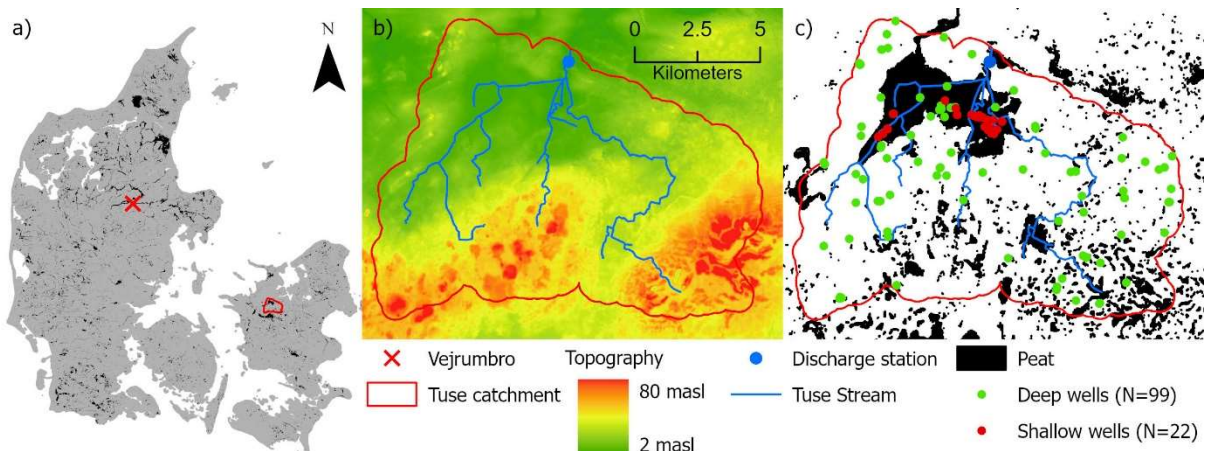
91 Of the studies applying fully integrated unsaturated-saturated flow models for peatland hydrology,
92 some focus on site or field-scale models (Friedrich et al., 2023; Haahti et al., 2015; Java et al., 2021;
93 Stenberg et al., 2018) while others apply the models at catchment scale (Ala-aho et al., 2017; Duranel
94 et al., 2021; Friedrich et al., 2023; Jutebring et al., 2018; Lewis et al., 2013). A catchment scale
95 approach with water balance closure is particularly important for climate change impact predictions,
96 since the boundary conditions to the peatlands will also be affected by climate change. Similarly, the
97 use of catchment scale models is important because impact evaluations of peatland management
98 scenarios, such as rewetting, can also include impacts on streamflow and groundwater levels in
99 neighboring areas.

100 The objectives of this study were to 1) estimate current and predict the future hydrology and soil CO₂
101 emissions in a Northern European drained peatland and 2) investigate the role of rewetting and
102 climatic extremes on annual CO₂ emissions. To achieve these objectives, we used a transient
103 physically-based hydrological 3D model to predict daily WTD for a case study area, the Tuse Stream
104 catchment, representing a typical degraded Danish peatland. Secondly, we developed an empirical soil
105 CO₂ flux (fCO₂) model based on coupled CO₂ flux, WTD and temperature observations for a similar
106 Danish peatland (Nielsen et al., 2025a), capable of making daily predictions. Combining the
107 mechanistic hydrological model and the empirical emission model enabled the estimation of daily soil
108 CO₂ fluxes under current conditions as well as scenarios of rewetting and future climate, while
109 accounting for the impact of climatic variability and extremes.

110 Data and methodology

111 Study area

112 Tuse Stream catchment is located on the island of Zealand in the eastern part of Denmark (Figure 1a).
113 The total area encompasses 107 km² of which 19 km² are peat soil. The areal extent of peat soil was
114 determined using a national map of organic soils (Adhikari et al., 2014). The largest continuous peat
115 area within the catchment is a 13 km² drained fen located in a river valley (Figure 1c) in the low-lying
116 part of the catchment. The peat soil area is primarily used for agriculture. In small parts of the area,
117 the drainage has been stopped to restore the natural hydrologic regime. The measured peat layer
118 thickness extends from 0.4 to 3.5 meters, below which alluvial sand deposits are typically found.
119 Generally, the deeper geology in the area can be characterized as clay-dominated glacial till deposits.
120 The catchment is characterized by flat topography, with the southern part of the catchment being
121 hillier. The climate conditions are humid and temperate. The catchment receives about 737 mm of
122 precipitation per year (1990-2024) and has an annual mean temperature of 9°C (Scharling, 1999a, b).



123

124 *Figure 1: a) Location of Tuse Stream catchment and the Vejrumbro site, b) topography and stream network of Tuse Stream*
 125 *catchment, masl: meter above sea level, c) location of organic soil and observation wells in the Tuse Stream catchment.*

126 Shallow WTD in the drained organic soils is monitored in 22 groundwater wells (2-3.5 meters deep)
 127 (Figure 1c). The wells are fully screened and WTD is automatically logged with pressure transducers at
 128 an hourly basis (aggregated to daily values) and verified with manual measurements. All WTD data are
 129 available in the Danish National Well Database (Jupiter, 2025). In this study, we define the water table
 130 depth (WTD) as positive when located below the surface and negative when above the surface.
 131 Monitoring data includes additional point measurements and timeseries of groundwater head from 99
 132 deep wells installed in mineral soils throughout the catchment (Figure 1c). In the model setup, water
 133 extraction in 40 abstraction wells is included based on data from the Danish National Well Database in
 134 May 2020 (Henriksen et al., 2020a) and implemented as yearly mean abstraction evenly distributed on
 135 the daily model timesteps. Daily discharge is monitored at the catchment outlet at Tuse Stream (Figure
 136 1b).

137 Hydrological modelling

138 The focus of the hydrological modelling in this study is to adequately simulate shallow groundwater
 139 levels and their dynamics for the peatland area in the Tuse Stream catchment. The fen peatland in
 140 Tuse Stream catchment is largely fed by groundwater discharge from the upstream catchment,
 141 emphasizing the need to develop a coupled groundwater surface water model at catchment scale. In
 142 addition, the objective of utilizing the model for climate change impact assessments requires a
 143 catchment scale approach with a deep groundwater component to represent changes in groundwater
 144 and surface water discharge to the peatland as well as changes in the boundary conditions. The
 145 catchment scale approach also facilitates the combined calibration and evaluation of the total water
 146 balance and peatland WTD by constraining the model with observed streamflow at the outlet as well
 147 as peatland groundwater level dynamics.

148 The model is set up as a transient, distributed, coupled surface-groundwater model and executed
 149 within the hydrological modeling framework MIKE SHE (DHI, 2022; Graham and Butts, 2005). MIKE SHE
 150 combines full 3D groundwater flow coupled with a gravity flow module in the unsaturated zone, 2D
 151 overland flow and 1D river flow routing in streams (DHI, 2019) (Figure S1). The simplified gravity flow
 152 module for unsaturated flow assumes a uniform vertical gradient and ignores capillary forces but
 153 provides a suitable solution for the time varying recharge to the groundwater table based on
 154 precipitation and evapotranspiration (DHI, 2022).

155 The model is a modified sub-model of the National Hydrological Model of Denmark (DK-model),
 156 developed at the Geological Survey of Denmark and Greenland (GEUS) (Henriksen et al., 2020a; Stisen
 157 et al., 2019). The geological model is interpreted in a horizontal 100 meter grid. The numerical model is

158 calibrated in the same 100 meter resolution, with the saturated zone consisting of 11 computational
159 layers of varying thickness. The top model layer has a uniform thickness of 2 meters, which is also
160 applied to the peat layer areas. The bottom level of the groundwater model is defined by the
161 prequaternary chalk that underlies the Island of Zealand, which in the Tuse Stream catchment is
162 located in a depth of approximately 150-250 meters below surface.

163 The time-varying constant head boundary conditions at the sub-model boundary are defined from the
164 operational National Hydrological Model setup (Henriksen et al., 2020b). The observed forcing data of
165 precipitation, temperature and reference evapotranspiration are provided by the Danish
166 Meteorological Institute (DMI) as gridded daily data in 10 km resolution for precipitation and 20 km
167 resolution for evapotranspiration and temperature (Scharling, 1999a, b; Stisen et al., 2011). The model
168 employs a maximum timestep of one day, at which the meteorological variables are fed into the
169 model. The model was provided with a hotstart file from an initial model run.

170 Spatial and temporal distributions of root depth and [leaf area index \(LAI\)](#) are based on classes (Figure
171 S2 and Table S1) where the peat, forest, agricultural and open nature land use classes have yearly
172 cycles of LAI and root depth (Figure S3). Likewise, soil type is spatially distributed (Figure S2) and based
173 on the three classes peat, sand and clay (Table S2). In the vertical direction, the soil columns in the
174 unsaturated zone module are divided into 40 cells from top to bottom; 30x0.1m, 5x1m and 5x5m.
175 Technically, the unsaturated zone is parameterized to 33 m depth, but during simulation limited to the
176 top of the simulated groundwater table. We implemented uniform vertical water retention
177 characteristics of peat, while clay and sand water retention characteristics were defined separately for
178 the depths 0-30 cm (horizon A), 30-70 cm (horizon B) and >70 cm (horizon C). Soil parameterization is
179 freely adapted from (Børgesen et al., 2009) and detailed in Table S3.

180 MIKE SHE allows incorporation of drainage systems, representing both artificial and natural drains. The
181 drainage system bypasses the slow water movement in aquifers by providing a short-cut from e.g. the
182 agricultural field to the nearest stream. The amount of water routed by drains from the saturated zone
183 to local surface water bodies is calculated using a linear reservoir model, where the difference
184 between groundwater head and drain level is multiplied by a drain time constant (dt). The drain level is
185 defined by a drain depth (dd) set relative to surface level. Hence, drainage in any given model cell only
186 occurs if the simulated groundwater level exceeds the drainage level (DHI, 2022). The drain time
187 constant and drainage depth in each model grid cell are distributed across the model domain
188 according to the five land use classes (Figure S2 and Table S1).

189 The model parameter sensitivity analysis and subsequent calibration prioritized parameters affecting
190 the shallow WTD in the peat soil and the overall water balance in the catchment. A list of model
191 parameters can be seen in Table S3. Parameter values not included in the calibration process are
192 obtained from the National Hydrological Model parametrization.

193 Calibration method

194 We used the Pareto Archived Dynamically Dimensioned Search (PADDS) algorithm (Asadzadeh and
195 Tolson, 2013) available within the optimization toolkit Ostrich (Matott, 2019). PADDS is a multi-
196 objective optimizer and obtains the pareto front across multiple objective function groups, enabling
197 post-weighting of individual objective functions. Throughout the calibration routine, Ostrich minimized
198 the weighted sum of squared error (WSSE) of each of the objective function groups. The PADDS
199 algorithm was run with the user settings of maximum 1000 iterations. The period 2010-2013 was used
200 as a calibration spin-up period and the model performance was evaluated for the 2014-2023
201 calibration period.

202 Calibration was performed against three objective function groups: $KGE_{WTD_modified}$, $r_{spatial}$ and
203 $KGE_qME_{head}ME_{amp}$ – as defined in Table 1. The $KGE_{WTD_modified}$ objective group is used to optimize the
204 model performance with respect to the WTD in peatlands. KGE is the Kling-Gupta Efficiency (Gupta et
205 al., 2009) and consists of three terms: the Pearson correlation coefficient r , a term representing the
206 measure of variability α and a bias term β (Table 1). In KGE , β is a unitless measure of the bias specified
207 as the ratio between the sum of simulated and observed values ($\beta = \frac{\sum sim - \sum obs}{\sum obs}$). As we use KGE to
208 optimize the WTD (and not hydraulic head), the operational sign can be both negative (water table
209 above surface/inundation) and positive (water table below surface), violating the idea of optimizing β
210 as the ratio of sums of values with possibly alternating operational signs. Therefore, we are using
211 $KGE_{WTD_modified}$ where β is replaced by the mean error (ME) (Table 1). This modification requires that the
212 order of magnitude of the ME_{WTD} is comparable to the errors on the other terms in KGE . In our case
213 this is ensured by the fact that the mean observed WTD values range between approximately 0.3-0.6
214 m, resulting in ME_{WTD} values typically below 0.5 m. Alternatively, the ME_{WTD} term could be scaled
215 within the KGE_{WTD} equation.

216 The calibration using the $KGE_{WTD_modified}$ as objective function group aims at achieving the best overall
217 agreement between simulated and observed WTD. However, during first calibration experiments, we
218 found that this objective function group primarily focuses on the temporal dynamics of WTD. To
219 improve the representation of the spatial variability of the mean WTD, the correlation coefficient
220 ($r_{spatial}$) was included as an additional objective function group (Table 1).

221 $KGE_qME_{head}ME_{amp}$ is an objective function group that combines three performance criteria: the Kling-
222 Gupta Efficiency performance criterion for discharge (KGE_q), the mean error of hydraulic head in
223 deeper aquifers (ME_{head}) and the mean error of annual amplitude of hydraulic head in the deeper
224 aquifers (ME_{amp}). For a detailed description of the implementation of ME_{amp} as objective function see
225 (Henriksen et al., 2020a). This objective function group was included to optimize the overall water
226 balance and streamflow dynamics expressed through the discharge at the catchment outlet (KGE_q), to
227 match the general water level in the deeper aquifers across the catchment (ME_{head}), and to match the
228 natural seasonal variations in hydraulic head (ME_{amp}). As the metrics of KGE_q , ME_{head} and ME_{amp} are
229 combined into one objective function group, we need to weigh the observations, to ensure that KGE_q ,
230 ME_{head} and ME_{amp} affect the objective group of $KGE_qME_{head}ME_{amp}$ approximately equally. This was done
231 based on WSSE from a model run with initial parameter values.

232

233

234

235

236

237

238

239

240

241

242 Table 1: Objective functions metrics. KGE stands for Kling-Gupta Efficiency.

Objective function group	Observations	No. of observation points wells	Metric	Abbreviation	Equation	Range	Optimum value
KGE _{WTD} _modified	Daily WTD in shallow wells (in peat)	22	Modified KGE on WTD	KGE _{WTD} _modified	$1 - \sqrt{(r_{WTD} - 1)^2 + (\alpha_{WTD} - 1)^2 + (ME_{WTD})^2}$ <i>r_{WTD} is the Pearson correlation coefficient between WTD_{sim} and WTD_{obs} pr. observation point, α_{WTD} = std_{WTD_sim}/std_{WTD_obs}, ME_{WTD} = 1/n ∑_{i=1}ⁿ WTD_{sim}_i - WTD_{obs}_i</i>	[-∞;1]	1
r _{spatial}	Mean WTD over the calibration period	22	Spatial correlation of the mean WTD	r _{spatial}	$r(WTD_{sim}, WTD_{obs})$ <i>r is the spatial Pearson correlation coefficient between mean WTD_{sim} and mean WTD_{obs} at 22 observation points</i>	[-1;1]	1
KGE _q ME _{head} ME _{amp}	Discharge	1	KGE on discharge	KGE _q	$1 - \sqrt{(r_q - 1)^2 + (\alpha_q - 1)^2 + (\beta_q - 1)^2}$ <i>r_q is the Pearson correlation coefficient between q_{sim} and q_{obs}, α_q = std_{q_sim}/std_{q_obs}, β_q = sum_{q_sim}/sum_{q_obs}</i>	[-∞;1]	1
	Hydraulic head in deep wells (in mineral soil)	66	Mean error on hydraulic heads	ME _{head}	$\frac{1}{n} \sum_{i=1}^n head_{sim_i} - head_{obs_i}$ <i>head_{sim} and head_{obs} are the average groundwater heads</i>	[-∞;∞]	0
			Mean error on yearly amplitude of hydraulic heads	ME _{amp}	$\frac{1}{n} \sum_{i=1}^n A_{sim_i} - A_{obs_i}$ <i>A_{sim} and A_{obs} are the annual amplitudes in groundwater head levels</i>	[-∞;∞]	0

243 WTD: water table depth [m], q: discharge [m s⁻¹], head: hydraulic head [m], A: amplitude [m]

244 A local sensitivity analysis based on initial parameter values from Table S4 was performed and values
 245 of composite scaled sensitivity (CSS) were obtained. Selection of free calibration parameters were
 246 based on the criterion that parameters were included if their CSS was larger than 0.05*CSS of the
 247 parameter with the highest CSS. The resulting 11 free parameters are indicated with grey in Table S4.
 248 Other parameters were kept at the values listed in Table S4 or tied to the calibration parameters.

249 Hydrological simulations of historical and future climate
 250 The calibrated hydrological model was run for the historical simulation period of 1990-2023 using
 251 observed climate forcing data (Scharling, 1999a, b; Stisen et al., 2011). Future hydrological projections
 252 are derived from simulations using the hydrological model forced by climate model projections,
 253 including precipitation, air temperature (T_{air}), and potential evapotranspiration. The resulting impacts
 254 on groundwater levels, as simulated by the hydrological model, are evaluated. We used 17 climate
 255 models (Table S5) with the Representative Concentration Pathway 8.5 (RCP8.5), which represents the
 256 RCP scenario (2.6-8.5) leading to the highest emissions and strongest impact of climate change. The
 257 climate model outputs are generated and bias corrected by (Pasten-Zapata et al., 2019), and the
 258 Global and Regional Circulation (GCM, RCM) models originate from the Euro-CORDEX project (Jacob et
 259 al., 2014).

260 The climate simulations cover three 30-year periods: the reference period (1991-2020), the mid-
 261 century (2041-2070) and the end-century (2071-2100). All 51 climate simulations (17 climate models ×
 262 3 periods) were first run using the initial potential head from the national model climate simulations
 263 (Henriksen et al., 2020a). Subsequently, they were rerun using the mean potential head for the
 264 respective 30-year period as the initial potential head.

265 Empirical CO₂ emission models

266 Implementation of annual CO₂ emission model

267 Recent studies established a functional relationship between the annual ~~net ecosystem carbon balance~~

268 {NECB} for CO₂ and the mean annual WTD (Koch et al., 2023; Tiemeyer et al., 2020) by fitting a

269 nonlinear Gompertz function. Like in (Koch et al., 2023; Tiemeyer et al., 2020), this study considers

270 NECB as only CO₂ fluxes, excluding methane (CH₄) and other carbon exports such as dissolved or

271 particulate organic carbon. We apply the WTD functional relationship for CO₂ from (Koch et al., 2023),

272 which is fitted to Danish flux data, and refer to it as the *Annual WTD model*. The *Annual WTD model*

273 demonstrates a systematic relationship in which CO₂ flux from NECB increases with annual WTD in the

274 interval between 7 cm and 50 cm, above which an asymptotic level of 10 Mg CO₂-C ha⁻¹ yr⁻¹ is reached

275 (Koch et al., 2023). The *Annual WTD model* is therefore not sensitive to changes in WTD deeper than

276 approximately 50 cm. At WTD levels less than 7 cm, the *Annual WTD model* suggests CO₂ uptake;

277 however, this element is not included in our analysis which only models CO₂ emission.

278 Derivation and implementation of daily CO₂ emission model

279 For our empirical model to predict daily soil CO₂ fluxes (fCO₂) we assume that the WTD dependent

280 NECB (Tiemeyer et al. 2020, Koch et al. 2023) is driven mainly by the response of soil respiration to

281 WTD and T_{air}, as gross primary photosynthesis (GPP) and aboveground autotrophic respiration is

282 mostly dependent on light availability and plant phenology (Rodriguez et al., 2024). This allows scaling

283 to match the NECB magnitude but maintains integrity in the regulation of WTD on soil CO₂ fluxes.

284 Using a unique and comprehensive coupled dataset (Nielsen et al., 2025a) of daily mean net soil CO₂

285 fluxes, T_{air} and WTD for six spatial replicate measurement points, we develop a coupled temperature

286 and WTD dependent empirical soil CO₂ flux model, hereafter referred to as the *Daily WTD-T_{air} model*.

287 The model essentially scales the WTD-fCO₂ relation to T_{air}. The dataset (Nielsen et al., 2025a) is from a

288 drained fen, called Vejrumbro (Figure 1), with similar characteristics (soil type, climate, land use

289 history) as the peat area in the Tuse Stream catchment (see methodological details in (Nielsen et al.,

290 2025a). The soil net CO₂ fluxes, WTD and T_{air} were measured automatically for one year (2022-2023)

291 (Nielsen et al., 2025a) and we used a subset of fluxes measured for six spatial replicates 5-6 times per

292 day, resulting in a dataset of 10950 – 13140 individual fluxes covering 365 days (Nielsen et al., 2025a).

293 Implementation of CO₂ flux models

294 Spatially distributed net soil CO₂ fluxes are calculated at a 100-meter scale across the 13 km²

295 contiguous peatland area (Figure 1) with the *Annual WTD model* and the *Daily WTD-T_{air} model*,

296 respectively, using WTD at a 100-meter scale (hectare scale) and a uniform T_{air}. Afterwards the

297 spatially distributed soil CO₂ fluxes are aggregated to represent the spatial mean of the 13 km²

298 peatland area.

299 First, we applied the *Annual WTD model* and the *Daily WTD-T_{air} model* for the historical simulation

300 period of 1990-2023, using spatiotemporal distributed WTD from the calibrated hydrological model.

301 Afterwards, the empirical CO₂ models are utilized on each of the 17 climate projections for T_{air} and

302 WTD. Daily T_{air} for the Tuse Stream catchment peatland area is taken directly from the 17 bias

303 corrected climate projections, while daily spatial WTD is a model output from the 17 hydrological

304 simulations, when running the hydrological model with the forcing data (precipitation, temperature

305 and evapotranspiration) from the 17 climate projections. Thereby, we are able to quantify the

306 variability in soil CO₂ flux among the 17 climate projections for each of the simulation periods and

307 among the 30 years within each of the simulation periods.

308 Design and application of rewetting scenarios
309 For impact evaluations of peatland management scenarios on the annual CO₂ emissions, we define
310 three rewetting scenarios: A, B and C. These scenarios are implemented through controlled
311 modifications of the simulated WTD in peatland grid cells. This method of representing rewetting
312 scenarios does not involve structural modifications to the hydrological model and assumes changes in
313 WTD without accounting for process-based feedback mechanisms within the coupled surface–
314 subsurface hydrological system. Therefore, the rewetting scenarios cannot be interpreted as real-life
315 management practices. All rewetting scenarios were applied for 1990 to 2023, representing the
316 climatology for this period and generating 34-year time series of rewetted WTD.

317 The scenarios are meant to illustrate different rewetting impacts on WTD, representing wetter winters
318 (A), uniform shift in WTD (B) and wetter summers (C), but all with the same long-term mean WTD. In
319 Scenario A, the daily groundwater table is elevated when it is above the long-term (34-year) mean
320 water table resulting in unchanged water table levels during summer but an increase in winter.
321 Scenario B uniformly raises the water table by a constant scalar, while Scenario C applies the same
322 scalar increase to water table while simultaneously reducing the annual amplitude by half. The
323 modifications of the simulated WTD are implemented using the following equations:

$$324 \quad WTD_{i,rewet\ A} = \begin{cases} WTD_i, & \text{if } WTD_i \geq \overline{WTD} \\ WTD_i + 2.5 \cdot (\overline{WTD} - WTD_i), & \text{if } WTD_i < \overline{WTD} \end{cases} \quad [2]$$

325

$$326 \quad WTD_{i,rewet\ B} = WTD_i - (\overline{WTD} - \overline{WTD_{rewet\ A}}) \quad [3]$$

327

$$328 \quad WTD_{i,rewet\ C} = \overline{WTD_{rewet\ B}} + 0.5 \cdot (WTD_{i,rewet\ B} - \overline{WTD_{rewet\ B}}) \quad [4]$$

329

330 where $WTD_{i,rewet\ A}$, $WTD_{i,rewet\ B}$ and $WTD_{i,rewet\ C}$ is the daily WTD in a grid cell for rewetting
331 scenario A, B and C, respectively. WTD_i is the daily WTD in a grid cell from the calibrated hydrological
332 model. \overline{WTD} is the long-term (34-year) mean WTD in a grid cell from the historical period of the
333 calibrated hydrological model. $\overline{WTD_{rewet\ A}}$ and $\overline{WTD_{rewet\ B}}$ are long-term (34-year) mean WTD in a
334 grid cell from the rewetting scenario A and B, respectively.

335

Uncertainty of Bootstrapping means of future climate CO₂ emission estimates

336 We applied a bootstrap resampling approach to estimate the uncertainty in the mean values of soil
337 CO₂ flux. Specifically, we resampled the means over the 17 climate models, each containing 30 annual
338 values, with replacement. This process was repeated 10,000 times to construct bias-corrected and
339 percentile-based 95% confidence intervals around the bootstrapped means.

340

341 Results

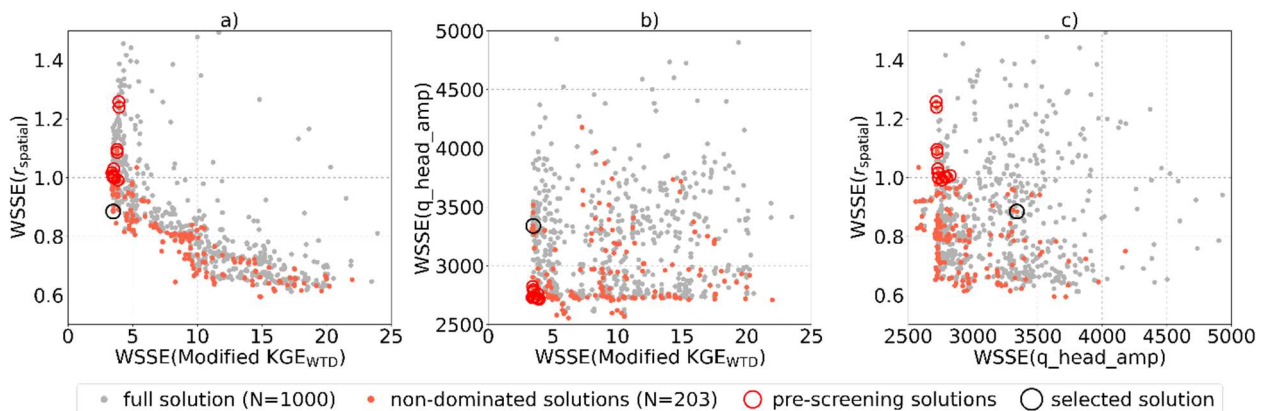
342 Hydrological model

343 Calibration of the hydrological model

344 The model calibration, running 1000 model evaluations based on three objective function groups,
 345 using Ostrich ParaPADDS optimizer with 40 parallel model executions, took ~24 hours on a Xeon E-
 346 4850 @2,20 GHz Server. The calibration resulted in 203 non-dominated solutions forming a three-
 347 dimensional pareto front. Figure 2 presents scatterplots of the three objective functions, illustrating
 348 the trade-offs between them. Especially, there is a clear trade-off between the two objective functions
 349 addressing temporal dynamics (KGE_{WTD}) and spatial dynamics ($r_{spatial}$), as illustrated in Figure 2a.

350 The number of non-dominated solutions and the trade-offs illustrate that several parameter sets can
 351 be considered and that an ensemble of parameter sets could be selected. For the purpose of further
 352 analysis and climate change impact assessments, however, we select one balanced solution from the
 353 non-dominated solutions, through a stepwise procedure. First, a pre-screening was performed with
 354 performance criteria for WTD of KGE_{WTD} larger than 0.6, for discharge of $KGE_{discharge}$ larger than 0.6 and
 355 for hydraulic head in deeper wells of ± 1 m, for ME_{head} and ME_{amp} , respectively. Afterwards, the
 356 balanced parameter set was selected as the solution with the highest spatial correlation ($r_{spatial}$).

357 The selection procedure was designed to prioritize accurate simulation of the temporal dynamics of
 358 peatland WTD, while maintaining strong performance across additional objective functions and
 359 maximizing spatial correlation accuracy. Initial calibration efforts indicated that achieving a KGE_{WTD}
 360 value greater than 0.6 was necessary to ensure an adequate alignment between the simulated and
 361 observed WTD time series.



362
 363 *Figure 2: Scatterplots of WSSE (weighted sum of squared errors) for the three objective function groups in the calibration.*
 364 *Pareto front for 1000 model evaluations.*

365 Hydrological model performance

366 Model performance metrics for the selected solution are summarized in Table 2. The q_head_amp
 367 objective function is separated into individual contributions from the metrics KGE_q , ME_{head} and ME_{amp} .
 368 Additionally, Table 2 shows the three metrics which make up the modified KGE_{wtd} : r_{wtd} , α_{wtd} and ME_{wtd} .
 369 In general, the model performs well with a KGE_{wtd} in peat of 0.64, a KGE_q of 0.63, a ME_{head} for the deep
 370 wells of 0.75 m and a ME_{amp} for the deep wells of 0.51 m for the selected solution. However, the
 371 correlation coefficient for the spatial variability ($r_{spatial}$) is poor with a value of 0.06. The model
 372 optimization achieves solid metrics on all the three components of KGE_{wtd} . The mean bias of WTD
 373 across all shallow peatland observation wells (ME_{wtd}) is only 8 cm (Table 2).

374 Table 2: Hydrological model performance

Name of metric	Abbreviation	Unit	Selected solution
Modified KGE on WTD	$KGE_{WTD,modified}$	-	0.64
Correlation coefficient WTD	r_{WTD}	-	0.83
Measure of variance	α_{WTD}	-	0.14
Mean error of WTD	ME_{WTD}	m	0.08
Spatial correlation of the mean WTD	$r_{spatial}$	-	0.06
KGE on discharge	KGE_q	-	0.63
Mean error on the hydraulic heads	ME_{head}	m	0.75
Mean error on amplitude of the hydraulic heads	ME_{amp}	m	0.51

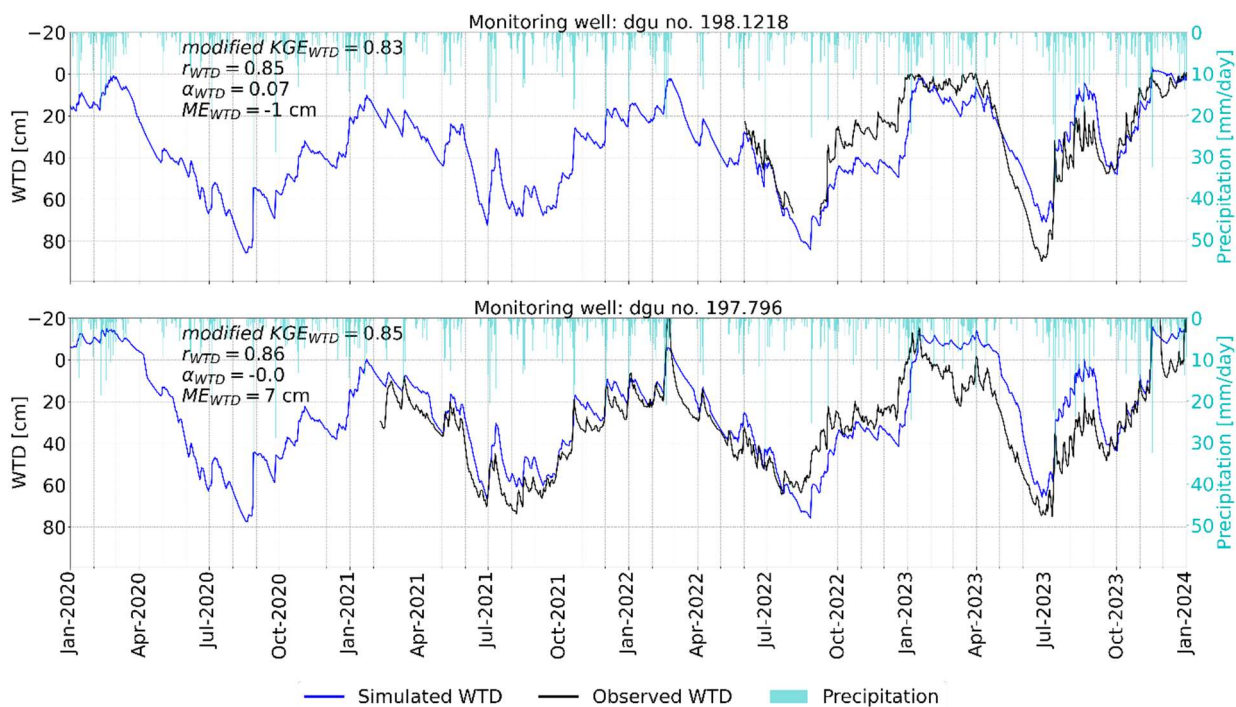
375

376 Though the model obtains a relatively small mean error, it largely underestimates the spatial variability
 377 in WTD. The observed mean WTD variability across the 22 monitoring wells ($SD = 16.5$ cm) is
 378 considerably higher than that observed in the simulations ($SD = 6.8$ cm). Even though the model
 379 performance on KGE_{WTD} was generally good, it proved difficult to reproduce the spatial variation in
 380 mean WTD.

381 To investigate the underestimation of spatial variability in WTD, we analyzed several spatial variables
 382 considered relevant for explaining the observed variability in WTD: peat thickness, topography and
 383 proximity to water bodies. However, no clear correlation was found between these spatial variables
 384 and the mean observed WTD or model bias, as all had a correlation coefficient smaller than 0.34. See
 385 Table S6.

386 Historical simulations of water table depth

387 The simulated WTD, generated by the calibrated hydrological model driven by historical climate for the
 388 period 1990-2023, adequately represent both the observed seasonal patterns of WTD and their short-
 389 term responses to precipitation events. Figure 3 shows the time series of WTD from two individual
 390 monitoring wells as a typical example of the temporal match between observed and simulated WTD.



391

392 Figure 3: Example of observed and simulated timeseries for water table depth (WTD) for monitoring wells dgu no. 198.1218
 393 and dgu no. 197.796. Including metrics for these wells.

394 Meteorological climate predictions
 395 Changes in precipitation, temperature and evapotranspiration patterns in future climate projections
 396 for Denmark generally indicate an increase in both temperature and annual precipitation. Table 3
 397 presents the mean air temperature, mean annual precipitation and mean potential evapotranspiration
 398 derived from the 17 climate projections across the three simulation periods.

399 *Table 3: Mean \pm SD (n=17) of annual air temperature, precipitation and potential evapotranspiration from the 17 climate*
 400 *models during the three simulation periods.*

	Unit	Reference period (1991-2020)	Mid-century period (2041-2070)	End-of-century period (2071-2100)
Mean annual air temperature	°C	8.9 \pm 0.7	10.6 \pm 0.8	12.1 \pm 0.8
Mean annual precipitation	mm yr ⁻¹	780 \pm 121	837 \pm 130	906 \pm 152
Mean annual potential evapotranspiration	mm yr ⁻¹	621 \pm 25	678 \pm 27	727 \pm 27

401

402 Hydrological climate predictions

403 Climate simulations using the hydrological model indicate a decreasing trend in mean annual WTDs
 404 (Table 4), resulting in a shallower annual mean groundwater table in future climate conditions. Both
 405 summer and winter mean WTDs are projected to be closer to the surface, suggesting generally wetter
 406 conditions. The mean annual amplitude of WTD remains unchanged under future climate scenarios
 407 (Table 4), indicating that there is no greater seasonal drawdown of the water table during summer,
 408 although the duration of the drawdown period may be extended.

409 *Table 4: Statistics of WTD when using the hydrological model for climate simulations. Mean \pm SD (n=17) over the 17 climate*
 410 *models during the three simulation periods. Summer is June, July and August, Winter is December, January and February. The*
 411 *amplitude is based on the monthly means of WTD to avoid outliers.*

	Unit	Reference period (1991-2020)	Mid-century period (2041-2070)	End -of-century period (2071-2100)
Mean annual WTD	cm	31 \pm 1	27 \pm 2	24 \pm 3
Mean summer WTD	cm	47 \pm 1	40 \pm 3	34 \pm 3
Mean winter WTD	cm	18 \pm 2	14 \pm 4	10 \pm 3
Mean annual WTD amplitude	cm	51 \pm 2	50 \pm 4	52 \pm 4

412

413 Derivation of empirical daily soil CO₂ flux model

414 An analysis of the Vejrumbro dataset indicated a clear temperature dependency on the relation
 415 between soil CO₂ flux (fCO₂) and WTD. The Vejrumbro dataset was resampled to daily means of WTD,
 416 T_{air} and soil CO₂ flux across the six spatial replicate measurement points omitting data from days with
 417 less than 24 flux measurements. This resulted in a dataset with 231 daily observations for each of fCO₂,
 418 WTD and T_{air} distributed evenly over a year. Traditionally, empirical emission models for ecosystem
 419 respiration (R_{eco}) are fitted to soil temperature. However, due to the strong linear relationship
 420 between daily soil temperature and daily air temperature at the Vejrumbro site ($r = 0.96$, p-value <
 421 0.001) (Figure S4), T_{air} was used as a proxy for soil temperature when fitting the *Daily WTD-T_{air} model*.
 422 This use of air temperature also facilitates upscaling and omits the need for projecting soil
 423 temperatures under climate change scenarios.

424 To investigate how the WTD-fCO₂ relation scales with temperature, we binned daily soil CO₂ flux into
 425 five temperature intervals: <4°C (n=39), 4-8°C (n=32), 8-12°C (n=52), 12-16°C (n=70) and >16°C (n=38)
 426 and applied a linear regression model ($y=ax$) with the intercept constrained at zero within each
 427 temperature bin. The regressions were constrained to pass through the origin, reflecting the

428 assumption that soil CO_2 flux is zero when the WTD is zero. Thereby, the relationship between $f\text{CO}_2$
 429 and WTD within each temperature bin was modeled using a linear regression of the form:

430 $f\text{CO}_2 = a \cdot \text{WTD}$ [5]

431 where $f\text{CO}_2$ represents soil CO_2 flux [$\text{Mg CO}_2\text{-C ha}^{-1} \text{ day}^{-1}$], a denotes the fitted slope and WTD is water
 432 table depth [cm], with positive values indicating depths below the surface.

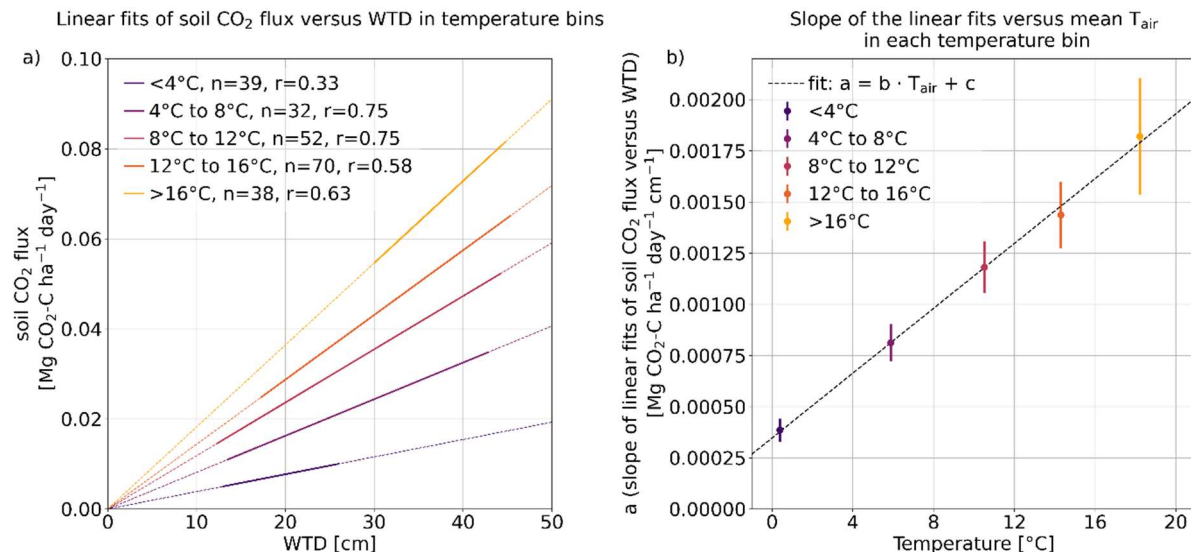
433 This analysis revealed an increasing slope, i.e. sensitivity of soil CO_2 flux to changes in WTD, with rising
 434 temperature (Figure S5 and Figure 4a), indicating that the WTD- $f\text{CO}_2$ slope (a) can be modelled as a
 435 linear function of temperature (T_{air}) (Figure 4b):

436 $a = b \cdot T_{\text{air}} + c$ [6]

437 Combining these relationships yields a simple model of the soil CO_2 flux:

438 $f\text{CO}_2 = b \cdot T_{\text{air}} \cdot \text{WTD} + c \cdot \text{WTD}$ [7]

439 where T_{air} [$^{\circ}\text{C}$] is the temperature, b [$\text{Mg CO}_2\text{-C ha}^{-1} \text{ day}^{-1} \text{ cm}^{-1} \text{ }^{\circ}\text{C}^{-1}$] and c [$\text{Mg CO}_2\text{-C ha}^{-1} \text{ day}^{-1} \text{ cm}^{-1}$] are
 440 empirical constants.



441

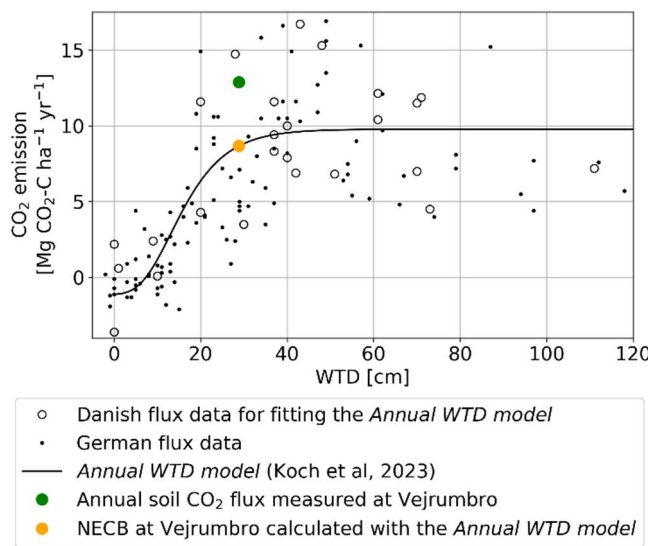
442 Figure 4: Left: linear models of soil CO_2 flux vs. water table depth (WTD) in air temperature bins. The thicker segment of the
 443 line represents the range of data used to derive the fitted model. n is the number of daily observations of soil CO_2 flux in each
 444 temperature bin. r is Person correlation coefficient. Raw data behind the linear regressions can be seen at Figure S5. Right:
 445 Slope (incl. uncertainty) (of the linear fit of soil CO_2 flux versus WTD) versus observed mean temperature in each temperature
 446 bin.

447 Having established a suitable form of the empirical soil CO_2 flux equation, we used nonlinear least
 448 squares fit to estimate the b and c parameters based on the daily soil CO_2 flux, T_{air} and WTD (without
 449 temperature bins). This method minimizes the residual sum of squares between the observed soil CO_2
 450 flux and the *Daily WTD-T_{air} model*. The resulting fitted model demonstrated a significant correlation to
 451 the observed data ($r = 0.78$, p -value < 0.001, $\text{RMSE} = 0.021 \text{ Mg CO}_2\text{-C ha}^{-1} \text{ day}^{-1}$) (Figure S6) with daily
 452 soil CO_2 flux increasing in response to rising WTD and T_{air} (Figure S7). The fitted empirical constants are
 453 as follows: $b = 8.32 \cdot 10^{-5} \text{ Mg CO}_2\text{-C ha}^{-1} \text{ day}^{-1} \text{ cm}^{-1} \text{ }^{\circ}\text{C}^{-1}$, $c = 3.33 \cdot 10^{-4} \text{ Mg CO}_2\text{-C ha}^{-1} \text{ day}^{-1} \text{ cm}^{-1}$.

454 The *Daily WTD-T_{air} model* predicts the highest soil CO_2 flux under conditions of simultaneously high T_{air}
 455 and WTD, where a high WTD refers to a water table located furthest below the surface (dry
 456 conditions). The multiplicative *Daily WTD-T_{air} model* demonstrated a moderate fit to the soil CO_2 flux
 457 data, with a R^2 of 0.61. To assess the individual contributions of the predictor variables, we also

458 computed the R^2 between CO₂ flux and T_{air} and WTD separately. This was done using a constructed
 459 dataset that included all combinations of WTD and T_{air} within the model range. This resulted in R^2
 460 values of 0.34 for T_{air} and 0.54 for WTD (Table S7). These values reflect the explanatory power of each
 461 variable in isolation.

462 Despite the significant variability in the observed ~~net ecosystem carbon balance~~ (NECB) used for the
 463 *Annual WTD model* (Figure 5) it is considered to represent a robust mean as it is based on multiple
 464 sites and years for Danish and German conditions. Compared to the *Annual WTD model* both the
 465 measured soil CO₂ flux (12.9 Mg CO₂-C ha⁻¹ yr⁻¹ (green circle)) and the *Daily WTD-T_{air}* simulated soil CO₂
 466 flux (13.6 Mg CO₂-C ha⁻¹ yr⁻¹ (not shown)) at Vejrumbro are above the corresponding fitted value of
 467 NECB (8.7 Mg CO₂-C ha⁻¹ yr⁻¹ (orange circle)) based on an annual WTD of 29 cm, but still within the
 468 range of observed NEBCs used for fitting the *Annual WTD model* (Figure 5). This may be explained by
 469 the methodology of flux measurements at Vejrumbro that did not consider GPP (CO₂ uptake) and
 470 therefore are expected to result in higher net CO₂ fluxes. In order to align the *Daily WTD-T_{air} model* to
 471 the level of the *Annual WTD model* where GPP is included, a scaling factor based on the above
 472 differences ($f_{scaling} = 0.64$) was applied to equation 7 to account for lack of GPP in the soil CO₂ fluxes
 473 used for empirical model development. Applying this scaling factor, we seek to avoid the risk of
 474 overestimating emissions when applying the *Daily WTD-T_{air} model* at other locations.



475
 476 *Figure 5: The Annual WTD model together with the Danish flux data of annual NECB and WTD data underlying the model*
 477 *(Koch et al., 2023). German flux data are included for comparison (Tiemeyer et al., 2020). Colored circles are measured and*
 478 *calculated soil CO₂ flux and NECB for the Vejrumbro dataset, so the colored circles represent the year 2022-2023.*

479 The Vejrumbro dataset used for fitting the *Daily WTD-T_{air} model* was limited to a maximum WTD of 47
 480 cm and maximum T_{air} of 21°C (Figure S7). Outside this range, the predictions of the *Daily WTD-T_{air}*
 481 *model* exhibits increased uncertainty. At the same time, it is generally understood that the upper
 482 portion of the peat layer drives the net CO₂ emissions observed at the surface. Therefore, the
 483 extrapolation of WTD in the *Daily WTD-T_{air} model* must be constrained. The *Daily WTD-T_{air} model*
 484 should be sensitive within a WTD range comparable to the expected daily variation in the *Annual WTD*
 485 *model*, which also reaches an fCO₂ asymptotic at deeper water tables. In the *Annual WTD model*, the
 486 Annual NECB reaches 90% of its maximum asymptotic level at a mean annual WTD of 30 cm (Figure 5).
 487 The mean annual WTD results from intra-annual (within year) WTD variation described by the annual
 488 amplitude. The mean annual amplitude (based on monthly means) is 65 cm, across the 22 observed
 489 WTD time series in the Tuse Stream catchment used for calibrating the hydrological model. We
 490 assume that a mean annual WTD of 30 cm originates from an annual WTD variation with a similar

491 amplitude. Therefore, we assume that the WTD range of the *Daily WTD-T_{air} model* is $30 + 65/2$ cm =
492 62.5 cm. For the T_{air} range, it is assumed that the sensitivity continues until 25°C, which is a daily
493 average value very rarely occurring, even in future climate projections. Thus, when applying the *Daily*
494 *WTD-T_{air} model*, daily WTD values and T_{air} values were truncated, setting WTD and T_{air} to 62.5 cm and
495 25°C, respectively, when exceeding those thresholds.

496 In both the *Daily WTD-T_{air} model* and the *Annual WTD model*, CO₂ fluxes are constrained so that the
497 model does not simulate negative fluxes or carbon uptake (Gyldenkærne et al., 2025).

498 CO₂ emissions from peatlands

499 CO₂ emissions throughout the historical simulation period

500 The long-term mean of the emission factor for the Tuse Stream catchment peat area is 8.0 ± 0.8 Mg
501 CO₂-C ha⁻¹ yr⁻¹ (mean \pm SD, n=34) when using the *Annual WTD model* and 8.8 ± 1.6 Mg CO₂-C ha⁻¹ yr⁻¹
502 (mean \pm SD, n=34) when using the *Daily WTD-T_{air} model* (Table 5).

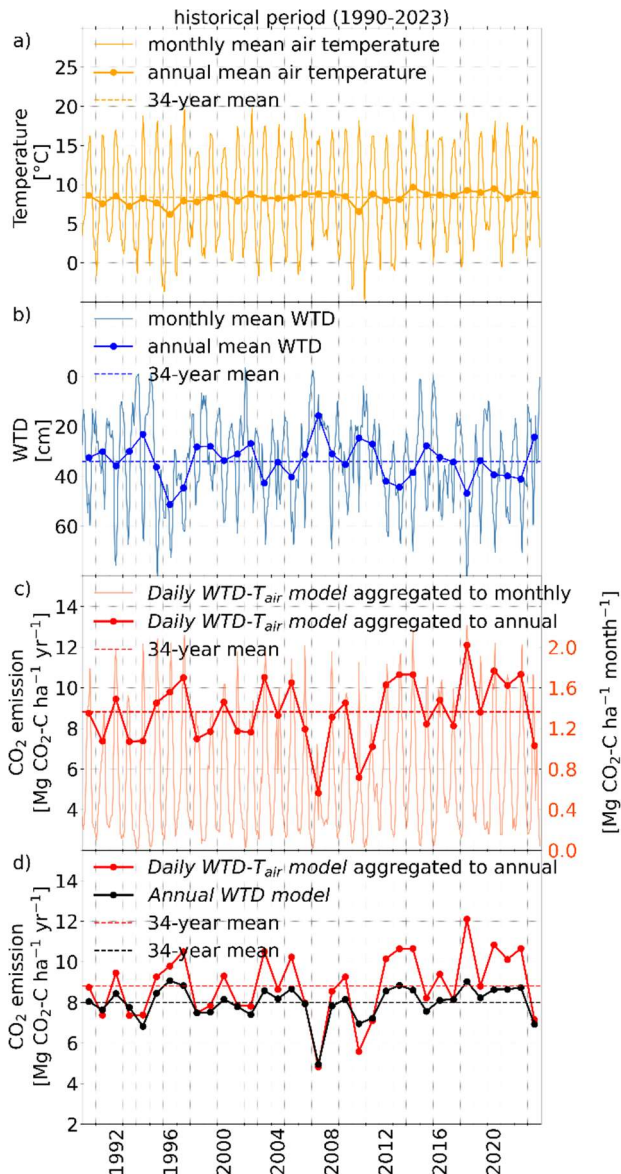
503 *Table 5: Long-term mean water table depth (WTD), long-term mean annual WTD amplitude (based on monthly means of WTD
504 to avoid outliers) and long-term soil CO₂ flux, throughout the historical period and the three modified 34-year WTD time series
505 of rewetting scenarios. Mean \pm SD is based on the 34 years of the historical period (1990-2023).*

	Unit	Historical period (1990-2023)	Rewetting scenario A	Rewetting scenario B	Rewetting scenario C
Mean WTD	cm	34 ± 8	14 ± 18	14 ± 8	14 ± 4
Mean annual WTD amplitude	cm	51 ± 11	110 ± 28	51 ± 11	26 ± 5
CO ₂ emission from <i>Daily WTD-T_{air} model</i> aggregated to annual	Mg CO ₂ -C ha ⁻¹ yr ⁻¹	8.8 ± 1.6	7.7 ± 2.0	5.2 ± 1.5	4.4 ± 0.8
CO ₂ emission from <i>Annual WTD model</i> aggregated to annual	Mg CO ₂ -C ha ⁻¹ yr ⁻¹	8.0 ± 0.8	4.6 ± 3.0	4.3 ± 2.0	4.4 ± 1.2

506
507 Figure 6 shows T_{air}, as well as the spatial mean of WTD and CO₂ emissions across the peatland, as
508 simulated by the *Daily WTD-T_{air} model* and the *Annual WTD model* during the historical period. The
509 CO₂ emissions calculated with the *Daily WTD-T_{air} model* (red line in Figure 6c, 6d) depend on both the
510 observed daily temperature variability (orange line in Figure 6a) and simulated intra-annual (seasonal)
511 WTD variability (blue line in Figure 6b), while the CO₂ emission calculated with the *Annual WTD model*
512 (black points in Figure 6d) only depends on the inter-annual (annual means) WTD (blue points in Figure
513 6b) and not the temperature.

514 Inter-annual (between years) variation in CO₂ emission is substantially larger when using the *Daily*
515 *WTD-T_{air} model* ($SD = 1.6$ Mg C-CO₂ ha⁻¹ yr⁻¹) compared to the *Annual WTD model* ($SD = 0.8$ Mg C-CO₂
516 ha⁻¹ yr⁻¹) (Figure 6d), as the former captures extreme events, such as periods of high temperature or
517 deep groundwater tables, as well as compound events involving the simultaneous occurrence of both.
518 In contrast, the *Annual WTD model* is insensitive to temperature and the intra-annual (within year)
519 timing of deep WTD. Moreover, the *Annual WTD model* imposes an upper limit of 10 Mg CO₂-C ha⁻¹
520 yr⁻¹ for annual emissions (Koch et al., 2023) (Figure 5). During the summer of 2018, a compound
521 extreme event occurred, characterized by both high temperatures and deep groundwater table. The
522 annual CO₂ flux for this year shows a 34% increase when estimated using the *Daily WTD-T_{air} model*
523 compared to the *Annual WTD model*. This discrepancy arises from the *Daily WTD-T_{air} model*'s ability to
524 account for the prolonged duration of concurrent high temperatures and deep groundwater table
525 conditions throughout the summer (Figure 6d). Conversely, in 2010, the *Daily WTD-T_{air} model*
526 estimates significantly lower annual CO₂ emissions compared to the *Annual WTD model* (Figure 6d).
527 This difference is due to the emission model's ability to account for the effects of prolonged periods of
528 low temperatures during the autumn and spring of 2010, leading to a mean annual temperature below

529 the long-term mean, despite summer temperatures being consistent with other years (Figure 6a).
 530 Examples of years with extreme events primarily driven by either WTD or T_{air} include 1996, which
 531 experienced a significant summer decline in groundwater table (Figure 6b), and 1997, which was
 532 characterized by elevated summer temperatures (Figure 6a). However, neither of these events led to
 533 CO_2 emissions as high as those simulated during the compound event of both high temperatures and
 534 deep water table in 2018 (Figure 6).



535
 536 *Figure 6: Air temperature (T_{air}), water table depth (WTD) and soil CO_2 emission for the historical simulation period 1990-2023.*

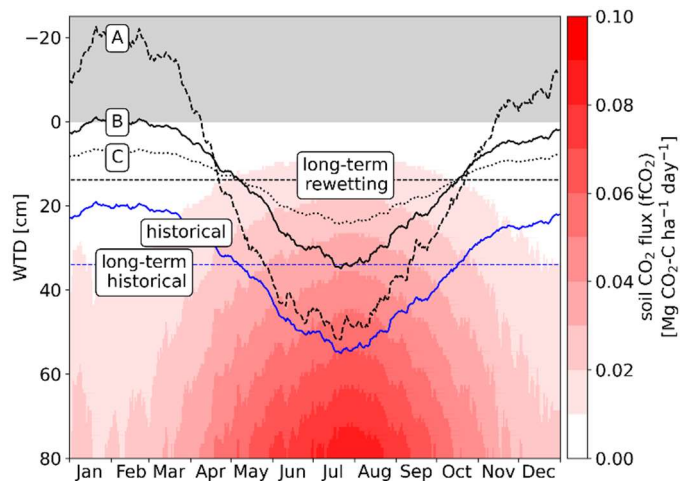
537 CO₂ emissions under different rewetting scenarios
 538 The rewetting scenarios represent an adjustment to the WTD simulated by the hydrological model
 539 over the 34-year historical period, thereby reflecting the climatological conditions prevailing during
 540 that time. Across all three rewetting scenarios, the long-term (34-year) mean WTD was raised by 20
 541 cm, from 34 cm to 14 cm below the surface, ensuring a consistent long-term annual mean WTD among
 542 the rewetting scenarios (Table 5). Accordingly, the application of the *Annual WTD model* for estimating
 543 CO₂ fluxes result in CO₂ emissions between 4.3 ± 1.2 Mg C-CO₂ ha⁻¹ yr⁻¹ (mean \pm SD, n=34) and 4.6 ± 3.0
 544 Mg C-CO₂ ha⁻¹ yr⁻¹ (mean \pm SD, n=34) across all rewetting scenarios (Table 5). The mean annual soil CO₂
 545 flux from the three rewetting scenarios, as calculated using the *Annual WTD model*, are similar but not

546 identical. This is because the *Annual WTD model* is applied to each of the 34 individual annual mean
547 WTD values rather than to a single long-term mean WTD. The SD of CO₂ emissions calculated using the
548 *Annual WTD model* in scenario C is markedly lower than in rewetting scenario A and B, reflecting the
549 lower inter-annual (between years) variability in mean annual WTD observed for this scenario (Table
550 5).

551 In contrast to the *Annual WTD model*, the *Daily WTD-T_{air} model* captures the simultaneous occurrence
552 of low groundwater table and high T_{air} during the summer months. Application of this emission model
553 indicates that raising the groundwater table during summer months (rewetting scenario C) yields the
554 greatest reduction potential in soil CO₂ emissions (Table 5), leading to a 50% decrease in the mean
555 value, from 8.8 ± 1.6 to 4.4 ± 0.8 Mg C-CO₂ ha⁻¹ yr⁻¹ (mean \pm SD, n=34) (Table 5). In contrast,
556 management scenarios that primarily target increase in winter water table (rewetting scenario A)
557 exhibit only marginal emission reduction potential (Table 5).

558 A visual representation of daily soil CO₂ emissions in relation to mean daily temperature during the 34-
559 year historical period under different WTD conditions (Figure 7) reveals that high summer
560 temperatures are a key driver of CO₂ emissions. WTD observations from the Tuse catchment peatland
561 indicate that, during shorter periods in the warm summer months, the WTD can exceed 80 cm (Figure
562 3). These periods with very low summer water table contribute substantially to total CO₂ emissions
563 (Figure 7).

564 A rewetting scenario that mainly generates wetter winter conditions (rewetting scenario A) has very
565 limited CO₂ emission reduction. All three scenarios assume that even under rewetting, the peatland
566 WTD will follow a climate driven seasonality and that obtaining zero WTD in summer periods will be
567 difficult by classical nature-based solutions. Rewetting scenario C, which features the greatest increase
568 in summer WTD, achieves the largest reduction in CO₂ emissions (Figure 7). Permanent wet conditions
569 with WTD at zero would be required to obtain zero CO₂ emission with the developed *Daily WTD-T_{air}*
570 *model*, but under such conditions, methane emissions would also come into play and plant growth
571 would be severely limited.



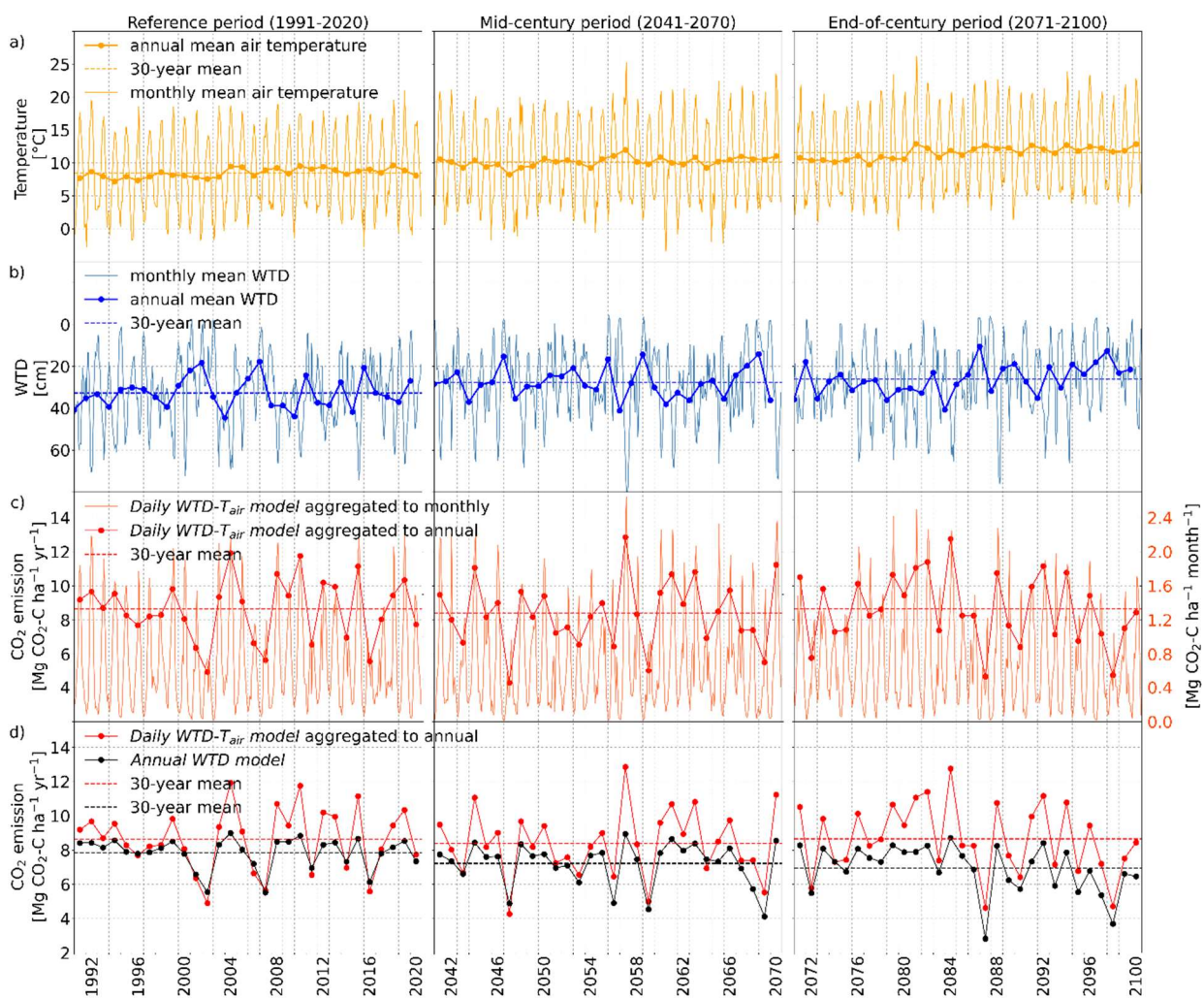
572
573 Figure 7: Colormap: Visual representation of the annual distribution of daily surface soil CO₂ flux (fCO₂, CO₂ exchange with
574 atmosphere) under mean daily temperature during the historical period (1990-2023) and for different water table depths
575 (WTD). Curves: solid blue line: simulated daily mean WTD during the historical period and corresponding long-term (34-year)
576 mean WTD, black lines: daily mean WTD for each of the modified 34-year WTD time series of rewetting scenarios (A, B and C)
577 and the corresponding long-term (34-year) mean WTD.

578 CO₂ emissions across future climate simulation periods
579 Figure 8 shows the same variables as Figure 6 but based on a representative climate model simulation
580 instead of the observed climate record, offering a typical example of the development of temperature,

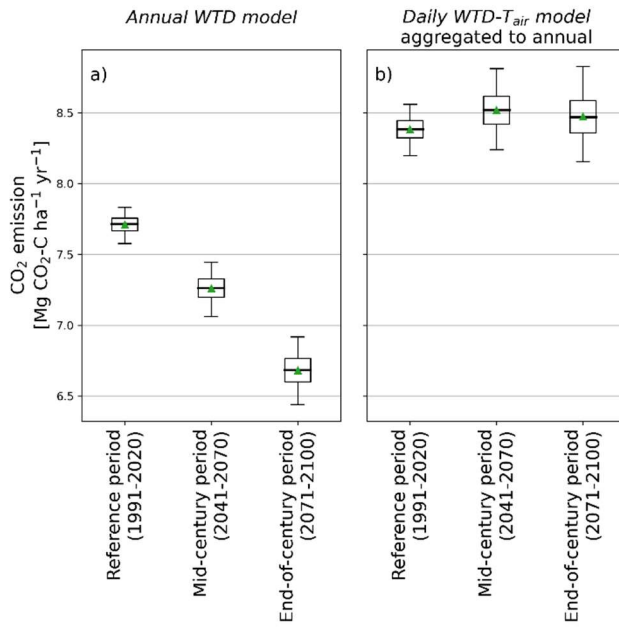
581 WTD and soil CO₂ flux through the reference, mid-century and end-of-century periods based on the
 582 RCP 8.5 pathway.

583 The future climate simulations show an increase in both the annual mean temperature and
 584 groundwater levels combined with higher maximum summer temperature (Figure 8a, 8b, Table 3,
 585 Table 4). The bootstrap mean of soil CO₂ flux calculated with the *Annual WTD model* over all climate
 586 models predicts a decreasing trend in soil CO₂ flux under future climate conditions (Figure 9a,
 587 horizontal dotted black line in Figure 8d), driven by an inter-annual (between years) mean WTD closer
 588 to surface (Table 4, Figure 8b). However, this decreasing trend is countered by the inclusion of T_{air}
 589 effects when applying the *Daily WTD-T_{air} model* (Figure 9b, horizontal dotted red line in Figure 8c and
 590 8d).

591 The wider confidence intervals in the mean annual CO₂ emissions for the future periods with both CO₂
 592 emission model (Figure 9) indicate that the inter-annual (between years) soil CO₂ fluxes become more
 593 variable in future climate. Furthermore, the confidence intervals for the individual periods are wider
 594 for the *Daily WTD-T_{air}* (Figure 9b) compared to the *Annual WTD model* (Figure 9a), which is expected as
 595 variations in T_{air} and not only WTD is included as with the *Daily WTD-T_{air} model*. This demonstrates that
 596 the *Daily WTD-T_{air} model* captures extreme events, including periods of high temperature or deep
 597 groundwater table, whether these events occur simultaneously (compound event) or independently.



598
 599 Figure 8: Example of air temperature (T_{air}), water table depth (WTD) and soil CO₂ flux for future climate simulation with
 600 climate model projection no. 5 (Table S6).



601
602 *Figure 9: Boxplot showing the distribution of bootstrap means of soil CO₂ emissions according to the Daily WTD-T_{air} model and*
603 *Annual WTD model during future climate. Green triangles and horizontal lines indicate the mean and the median of the*
604 *bootstrap mean, respectively. Boxes show the 25th and 75th percentiles. Whiskers indicate the 95% confidence intervals.*
605 *Outliers are not shown.*

606 The results presented in Figure 9 suggest that the impact on CO₂ emissions caused by future increases
607 in T_{air} and increases in water tables cancel each other out when using the *Daily WTD-T_{air} model*. To
608 investigate this further, we analyze how the combination of T_{air} and WTD shift between the reference
609 and the end-of-century periods, despite relatively stable total CO₂ emission.

610 We wish to identify the specific combination of T_{air} and WTD that are associated with the majority of
611 the CO₂ emission. Due to the non-linear response of soil CO₂ flux to environmental drivers in the *Daily*
612 *WTD-T_{air} model*, a large fraction of total emissions is generated on relatively few days. To quantify this,
613 we calculated p50, defined as the proportion of days required to account for 50% of the total annual
614 soil CO₂ flux (fCO₂). This was achieved by ranking the daily values of fCO₂, WTD, and T_{air} in ascending
615 order according to fCO₂. Subsequently, the ranked fCO₂ values were cumulatively summed to obtain
616 their percentile distribution (Figure S8). The procedure was first applied to fCO₂, WTD, and Tair data
617 from the historical simulation period, with the resulting percentile curves shown in Figure S8. Over the
618 historical simulation period, 50% of the total fCO₂ (fCO_{2,p50}) was generated within 22% of the days (p50
619 = 22%), while the value of fCO_{2,p50} and corresponding WTD_{p50} and T_{air,p50} are estimated to be 4.15·10⁻²
620 g CO₂-C ha⁻¹ day⁻¹, 47 cm and 13.8 °C (Table 6 and Figure S8).

621 Similar estimates are derived from the three timeslots from the climate models (reference, mid-
622 century and end-of-century climate simulation periods) using the 17 different climate models. For the
623 future, 50% of the total fCO₂ is expected to occur within approximately 21 ± 1 % (mean ± SD, n=17) of
624 the days (Table 6). The daily soil CO₂ flux associated to p50 (fCO_{2,p50}) and p50 are nearly identical
625 across both the historical and future climate simulations periods (Table 6). As also shown in Figure 9b,
626 the magnitude and temporal distribution of fCO₂ are predicted to remain unchanged in the future.
627 While the value of fCO_{2,p50} remains relatively constant around 4·10⁻² Mg CO₂-C ha⁻¹ day⁻¹ for future
628 climate periods, the corresponding WTD_{p50} and T_{air,p50} values change as a result of changing climate
629 moving towards higher temperatures (17 °C) and shallower groundwater table (40 cm).

630 Figure 10 provides a graphical representation of fCO₂ obtained from the *Daily WTD-T_{air} model*, with the
631 colormap illustrating the daily fCO₂ corresponding to different combinations of T_{air} and WTD. The daily

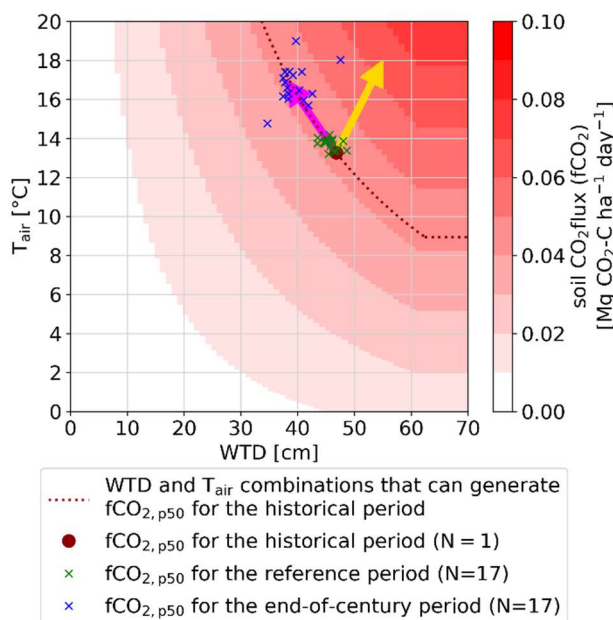
632 $fCO_{2, p50}$ ($4.15 \cdot 10^{-2}$ g $CO_2\text{-C ha}^{-1} day^{-1}$ for the historical period (Table 6)) can be achieved through
 633 various combinations of T_{air} and WTD (dark red dotted line in Figure 10). The values of $T_{air, p50}$ and
 634 WTD_{p50} corresponding to $fCO_{2, p50}$ for the Tuse Stream catchment peatland are plotted as a dark red
 635 point. As expected, the $fCO_{2, p50}$ values for the reference periods of the 17 climate models (green
 636 crosses at Figure 10) are closely aligned with that of the historical period. It is evident that the $fCO_{2, p50}$
 637 values for the end-of-century climate conditions (blue crosses at Figure 10) shift along the direction
 638 indicated by the pink arrow (along the red dotted line), reflecting a trend toward higher temperatures
 639 and lower WTD (i.e. water levels closer to the surface surface). This indicates that the mean daily fCO_2
 640 (Table 6) and the long-term fCO_2 remains constant in the future (Figure 9b), as a result of a
 641 counterbalance between impacts of rising temperatures and rising groundwater levels.

642 The pink arrow at Figure 10 illustrates the characteristic impact of climate change in Denmark,
 643 reflecting the concurrent increase in air temperature and shallow groundwater levels (Schneider et al.,
 644 2022). In contrast, other regions in Europe are experiencing declining groundwater level trends to
 645 climate change (Wunsch et al., 2022). Consequently, CO_2 emissions from peatlands in these regions
 646 are expected to shift in the direction indicated by the yellow arrow in Figure 10, towards considerably
 647 larger emission rates.

648 *Table 6: p50 is the fraction of days required to reach 50% of the total soil CO_2 flux (fCO_2). $fCO_{2, p50}$ is the daily soil CO_2 flux
 649 associated with p50. WTD_{p50} and $T_{air, p50}$ are the water table depth (WTD) and air temperature (T_{air}) corresponding to $fCO_{2, p50}$,
 650 respectively. Mean \pm SD is based on 17 climate model simulations.*

	Unit	Historical simulation period (1990-2023)	Climate simulation periods		
			Reference period (1991-2020)	Mid-century period(2041-2070)	End-of-century period (2071-2100)
p50	% days	22	21 ± 1	21 ± 1	21 ± 1
$fCO_{2, p50}$	$Mg\ CO_2\text{-C ha}^{-1} day^{-1}$	$4.15 \cdot 10^{-2}$	$4.03 \cdot 10^{-2} \pm 9.89 \cdot 10^{-4}$	$4.00 \cdot 10^{-2} \pm 3.24 \cdot 10^{-3}$	$4.03 \cdot 10^{-2} \pm 3.65 \cdot 10^{-3}$
$T_{air, p50}$	°C	13.8	14 ± 0.3	15 ± 0.6	17 ± 1.0
WTD_{p50}	cm	47	46 ± 1	42 ± 3	40 ± 3

651



652 *Figure 10: Colormap: Visual representation of the Daily WTD- T_{air} model output, illustrating soil CO_2 flux (fCO_2) as function of
 653 daily water table depth (WTD) and air temperature (T_{air}). The dark red dotted line represents combinations of T_{air} and WTD
 654 that corresponds fCO_2 at $p50$ ($fCO_{2, p50}$), where $p50$ is the fraction of days required to reach 50% of the total accumulated fCO_2
 655 during the historical period. Green crosses are $fCO_{2, p50}$ for the reference period of the 17 climate simulations. Purple crosses
 656 during the historical period. Green crosses are $fCO_{2, p50}$ for the reference period of the 17 climate simulations. Purple crosses*

657 are $fCO_{2, p50}$ for the end-of-century climate simulation period of the 17 climate simulations. The pink and yellow arrows
658 indicate different future trends in T_{air} and WTD and the associated trend in CO_2 emissions under climate change. Specific to
659 Denmark, the pink arrow indicates increases in T_{air} and decrease in WTD, other regions might experience increase in both T_{air}
660 and WTD and an associated large increase in CO_2 emissions (yellow arrow).

661 Discussion

662 Peatland management under changing climate

663 In 2023, CO₂ emissions from drained organic soils in croplands and grasslands was estimated to have
664 accounted for 6.7% of Denmark's total emissions, including those from the Land Use, Land-Use Change
665 and Forestry (LULUCF) sector (Nielsen et al., 2025b). Returning peatland organic soils to their natural
666 hydrological state is a cost-effective GHG reduction strategy (IPCC, 2014; Kirpotin et al., 2021;
667 Tanneberger et al., 2021; Wilson et al., 2016). Therefore, national policies (Regeringen, 2024) and the
668 European Union's Nature Restoration Law (Regulation (EU) 2024/1991, 2024) seek to improve the
669 management of peatlands and achieve climate neutrality targets under the urgent Green Transition
670 agenda. To mitigate agricultural GHG emissions Danish ministerial agreements were initiated in 2024,
671 targeting the restoration of 140,000 hectares of peatland. [Moreover, a CO₂-eq tax on emissions from
672 organic peatlands is scheduled for implementation from 2028](#) (Regeringen, 2024). However, there is a
673 need to strengthen the scientific evidence for mitigation measures to facilitate cost-effective policies.

674 Integration of the process-based hydrological model of the Tuse Stream catchment with the
675 empirically derived *Daily WTD-T_{air} model* of soil CO₂ flux developed in this study revealed that emission
676 simulations at daily timesteps produce greater variability in soil CO₂ fluxes compared to emission
677 estimates derived from annual WTD means. This increased variability is attributed to the daily model's
678 ability to account for short-term compound events, especially the simultaneous occurrence of elevated
679 air temperatures and low groundwater levels.

680 More importantly, incorporating temperature dependence and higher temporal resolution into the
681 CO₂ emissions model significantly alters the projected trends of CO₂ emission under both rewetting
682 and changing climate conditions.

683 [Nature-based approaches represent the most common real-world rewetting strategies, aiming to
684 restore peatlands towards their natural hydrological regime. At a minimum, such rewetting requires
685 terminating tillage activities and eliminating artificial drainage for instance by blocking of drainpipes
686 and ditches. The rewetting scenarios implemented in this study, represented as simple modifications
687 to WTD, are not reflective of practical management interventions - except perhaps in a few rare and
688 costly restoration projects that involve installing artificial impermeable membranes along peatlands
689 edges](#) (Naturstyrelsen, 2022). [However, the outcome of this study can inform discussions on
690 requirements and best practices for rewetting and peatland restoration. The study also highlights the
691 need to monitor or model pre- and post-restoration WTD dynamics in order to develop realistic
692 expectations regarding CO₂ emission reductions from rewetted peatlands](#) [However, the outcome of
693 this study can serve as a reference for discussions on realistic expectations on CO₂-emission reductions
694 from rewetted peatlands.](#)

695 The rewetting analyzed in this study showed how different rewetting scenarios with varying seasonal
696 amplitudes in WTD suggest significantly different emission reduction potential even with identical
697 annual mean WTD. The results illustrate that increasing the groundwater table during warm periods is
698 key to obtaining CO₂ emission reductions, whereas rewetting strategies that mainly raise winter water
699 table without significantly affecting the summer levels offer limited mitigation benefits. This highlights
700 the importance of not only targeting annual reductions in WTD but particularly designing rewetting
701 strategies to increase the summer water table and avoid critically low water levels during droughts and
702 warm periods. Achieving such rewetted conditions may include larger forced control of WTD than
703 what is currently being practiced for most existing rewetting schemes, where the WTD remain subject
704 to climate seasonality impact. Such nature-based solutions are not likely to reduce CO₂ emissions to
705 the degree that current emission reduction policies target.

706 Also, projections of CO₂ emissions under different climate change scenarios were altered greatly by
707 introducing temperature sensitivity and enhanced temporal resolution into the CO₂ emissions
708 modeling framework. Here our results show that, while the projected rise in groundwater tables in
709 isolation would lead to lower CO₂ emissions in future (when using the *Annual WTD model*), the *Daily*
710 *WTD-T_{air} model* revealed that anticipated increases in T_{air} are likely to cancel out these reductions,
711 resulting in CO₂ emissions on a level comparable to current levels. This is an important finding, since it
712 suggests that increasing temperatures alone will likely increase CO₂ emissions, and that water level rise
713 driven by climate change or rewetting initiatives might just counteract this trend. Rewetting measures
714 would need to be substantially intensified to ensure climate resilience and achieve meaningful
715 reductions in CO₂ emissions. Additionally, outside the specific case of Danish peatlands located in a
716 region that is susceptible to a future wetter climate, other regions might project both increasing
717 temperatures and lower groundwater tables, and in such cases climate change will significantly
718 increase emissions without any rewetting. We acknowledge that the chosen ~~Representative~~
719 ~~Concentration Pathway~~ (RCP8.5) represents the scenario leading to the strongest impact of climate
720 change and that additional, milder climate scenarios could have been included.

721 Hydrological simulation of groundwater levels in peat soil with process-based models
722 Existing large scale CO₂ emission estimates, such as national inventories from organic soils
723 (Gyldenkærne et al., 2025; Nielsen et al., 2025b), typically combine empirical emission models and
724 data-driven ML approaches for estimating annual WTD (Bechtold et al., 2014; Koch et al., 2023;
725 Tiemeyer et al., 2020). These approaches appear robust and suited for upscaling but are limited in
726 their ability to represent the impact of sub-annual variability in temperature and WTD, which are
727 issues that become increasingly important when analyzing effects of rewetting and climate change. In
728 contrast to most data-driven approaches, hydrological models enable a climate-driven representation
729 of WTD temporal dynamics and the underlying hydrological processes. Moreover, the use of physically
730 based hydrological models has the distinct advantage of enabling scenario-based analyses, such as the
731 evaluation of alternative land use strategies and the projection of future hydrological conditions under
732 climate change scenarios. Utilizing hydrological models that generate high-resolution time series of
733 WTD, it is possible to quantify impacts of WTD dynamics, including water levels, temporal variability
734 and seasonal amplitudes, on changes in CO₂ emissions.

735 That said we acknowledge that the rewetting scenarios in the present study are applied using
736 simplified adjustments to the simulated WTD, rather than being modeled through a detailed, process-
737 based hydrological framework. Ideally, future assessments should apply catchment-scale models to
738 evaluate peatland management interventions, such as rewetting, thereby enabling analysis of their
739 broader hydrological impacts, including effects on streamflow and groundwater levels in neighboring
740 areas. A unique feature of the present study is that the hydrological model of Tuse Stream catchment is
741 developed in the same modelling framework as the National Hydrological Model of Denmark
742 (Henriksen et al., 2020a; Stisen et al., 2019). The National Hydrological Model is continuously updated
743 with new data and operates in near real-time. This integration enables a link between the lessons
744 learned from the Tuse Stream catchment-scale model and the National Hydrological Model of
745 Denmark, thereby improving the representation of peatland hydrology and contributing to the
746 refinement of future national GHG inventories.

747 As a continuation of this study, we will further investigate the spatial variability of WTD and extent
748 hydrological model to include additional peatland-dominated catchments. Additionally, we will utilize
749 the National Hydrological model to simulate WTD across all Danish peatlands.

750 Selection, fit and transferability of daily CO₂ emission model
751 Detailed process-based terrestrial ecosystem models that simulate biogeochemical cycles and
752 vegetation are available (Bona et al., 2020; Oikawa et al., 2017; Wu and Blodau, 2013). Such modelling
753 schemes rely largely on multiple parameters related to plant and soil biogeochemistry which are not
754 generally attainable, thereby limiting the possibility to generalize and upscale.

755 As an alternative a range of empirical models with varying levels of complexity has been developed to
756 describe ecosystem respiration; however, the most commonly applied formulation is the Lloyd–Taylor
757 model (Lloyd J., Taylor, 1994), in which temperature acts as the sole independent variable. Structural
758 complexity in empirical equations is increased through the integration of various other environmental
759 variables, for example, hydrological variables such as WTD (Rigney et al., 2018). Recent alternative
760 empirical approaches for estimating CO₂ emissions for organics soils include response functions linking
761 average annual WTD to annual emissions (Arents et al., 2018; Evans et al., 2021; Tiemeyer et al., 2020),
762 such as the *Annual WTD model* (Koch et al., 2023) used in this study.

763 To evaluate alternative empirical emission models alongside our *Daily WTD-T_{air} model*, we fitted three
764 different empirical formulations from (Rigney et al., 2018) to the Vejrumbro soil CO₂ flux data (Table
765 S7). Each of the three empirical formulations incorporated both temperature and WTD as independent
766 variable. The model fitting resulted in R² values comparable to those obtained from fitting the *Daily*
767 *WTD-T_{air} model* developed in this study (Table S7).

768 Studying the explanatory power of each independent variable of WTD and T_{air} in isolation in the other
769 empirical emission models, revealed that models in which WTD and T_{air} are incorporated as additive
770 terms, rather than as interdependent (e.g., multiplicative) terms (as in eq. 6 and 8 in (Rigney et al.,
771 2018)), often exhibit coefficients of determination (R²) that are excessively dominated by either WTD
772 or T_{air} (Table S7). This indicates that such model formulations may inadequately capture the joint or
773 synergistic effects of these variables on the dependent variable. The challenge likely stems from the
774 fact that both WTD and T_{air} exhibit similar seasonal patterns, which may lead the regression to
775 primarily fit one of the additive terms containing either WTD or T_{air}. Empirical models that incorporate
776 WTD and T_{air} as multiplicative terms (such as equation 7 in (Rigney et al., 2018) and the *Daily WTD-T_{air}*
777 model developed in this study) demonstrate a more balanced distribution of explanatory power
778 between each independent variable (Table S7). Nevertheless, equation [7] in (Rigney et al., 2018)
779 remains predominantly influenced by the T_{air} component (Table S7). A more balanced distribution of
780 explanatory power between temperature and WTD is desirable, given that both variables are
781 recognized as key drivers of soil CO₂ flux dynamics, which is achieved better with the *Daily WTD-T_{air}*
782 than with any of the empirical models in Table S7.

783 We acknowledge that the *Daily WTD-T_{air} model* does not reproduce many of the highest observed fCO₂
784 values (Figure S6 and S7). In addition to identifying a relationship between fCO₂ and WTD, which was
785 used to derive the *Daily WTD-T_{air} model* (Figure S5), we studied the temperature sensitivity within
786 WTD bins to better understand the model's inability to reproduce the highest observed fCO₂ values.
787 Specifically, we binned the daily fCO₂ into four WTD intervals: <20 cm (n=73), 20 to 40 cm (n=37), 30 to
788 40 cm (n=77) and >40 cm (n=44) (Figure S9). We identified a potential relationship between fCO₂ and
789 temperature within WTD bins (Figure S9). This result is expected given the strong interdependence
790 among fCO₂, temperature and WTD, all of which exhibit comparable seasonal dynamics. The high
791 observed fCO₂ values cannot be captured by a simple empirical model based solely on T_{air} and WTD,
792 particularly because both high and low fCO₂ occur under similar T_{air} and WTD conditions (Figure S5, S7
793 and S9). Consequently, the *Daily WTD-T_{air} model* represents a compromise that captures part of the
794 variability while preserving a realistic mean response.

795 In this study, we demonstrate the need for the development of emission models operating on a sub-
796 annual timescale. It highlights the necessity of creating scalable generalized models based on
797 temperature, WTD and possibly other predictors. The development of such models requires data from
798 a large number of sites with continuous and temporally dense measurement, in order to integrate
799 information in a manner similar to models based on annual WTD. We recognize that currently, models
800 based on annual WTD are likely the most robust for upscaling to national level and current conditions.

801 The simulated soil CO₂ flux at Vejrumbro, estimated using the *Daily WTD-T_{air} model* (13.6 Mg CO₂-C ha⁻¹ yr⁻¹), aligns well with flux measurements from Danish and German sites (Figure 5). This agreement
802 suggests a comparable magnitude of emissions across geographically distinct locations of similar
803 characteristics, such as soil type and land use history.

804 We acknowledge that the *Daily WTD-T_{air} model* is derived from a single dataset, and that other
805 emission models also provide valid fits of WTD and T_{air}. Furthermore, we recognize that empirical
806 emission models are highly dependent on the specific data to which they are fitted. Acknowledging the
807 limited data behind the *Daily WTD-T_{air} model* utilized in this study, the goal has not been to accurately
808 estimate the peatland emission budget, which will be uncertain due to the reliance on a single site.
809 However, the objective has been to illustrate the impact and insights gained from applying emission
810 models at a daily timescale and how this has significant impact on the conclusions that can be made
811 regarding effects of rewetting and climate change. The decision to utilize the *Daily WTD-T_{air} model* for
812 rewetting and climate modeling scenarios is motivated by the simplicity of the relationship and its
813 direct derivation from the Vejrumbro data, which clearly demonstrates a temperature-dependent
814 relationship between soil CO₂ flux and WTD. The limited availability of multiple high-temporal-
815 resolution GHG emission datasets broadly restricts the ability to generalize and upscale empirical GHG
816 emission models at a daily timescale. Therefore, we consider the *Daily WTD-T_{air} model* to be the most
817 reliable option currently available. Future research should validate the performance of emission
818 models on intra-annual (within years) data with continuous measured CO₂ data.

819
820 A promising methodology for future applications, as well as for integrating a Tier 3 framework,
821 involves coupling a process-based hydrological model with process-based emission models or an
822 empirically derived daily emission model, such as the one developed in this study, to enable detailed
823 simulations of GHG emissions that capture short-term dynamics and compound environmental effects.

824

825

826 Conclusion

827 This study demonstrates the feasibility of simulating the temporal dynamics of the peatland water
828 balance and shallow groundwater table depth (WTD) using a catchment-scale distributed hydrological
829 model. Accurately modelling shallow WTD is critical for reliable projections of CO₂ emissions from
830 peatlands. We combined simulations of shallow WTD from the calibrated hydrological model with two
831 empirical CO₂ emission models 1) an annual WTD-CO₂ relationship and 2) a daily WTD-CO₂ model
832 accounting for the temperature effect on soil CO₂ production. This approach was used to estimate net
833 soil CO₂ emissions for the historical period (1991-2020), the mid-century period (2041-2070) and the
834 end-of-century period (2071-2100). This demonstrated that projections of soil CO₂ emissions are highly
835 sensitive to the complexity and temporal resolution of the emission model applied. Specifically,
836 models that incorporate both temperature and WTD dynamics at a daily timescale results in vastly
837 different conclusion regarding impacts of climate change and rewetting. Regarding climate change
838 impacts, we show that a daily temperature and WTD based emission model predict increased
839 emissions due to temperature changes, which can be counter balanced (in the Danish case) or
840 amplified depending on the future trend in WTD. Our results also demonstrate that rewetting
841 strategies aimed at raising the groundwater table during the warm summer period offer a CO₂
842 emission reduction potential of up to 50%, whereas approaches focused primarily on increasing winter
843 water table levels result in only marginal reductions. The combination of process-based hydrological
844 model simulations and a daily-resolution empirical CO₂ emission model used in this study captures the
845 influence of short-term compound climate events—such as simultaneous high temperatures and low
846 WTD—which substantially alters projected emission trends compared to simpler approaches. Such
847 refined approaches are essential for developing adaptive, climate-resilient peatland restoration
848 policies and improving national greenhouse gas inventories. The findings underscore the importance
849 of moving beyond static, annual WTD thresholds in peatland management by incorporating dynamic
850 hydrological simulations. Instead, rewetting strategies should prioritize maintaining elevated summer
851 groundwater table levels to buffer against drought-induced emission peaks.

852 Supplement link

853 ...

854 Author contributions

855 All authors contributed to the conception and design of the study. TD conducted the analysis and
856 drafted the manuscript, with input and revisions from all co-authors.

857 Competing interests

858 The authors declare that they have no conflict of interest.

859 Acknowledgements

860 We would like to thank Independent Research Fund Denmark for supporting the project PEAtlands and
861 Climate-driven variability in groundwater depth – Impacts on greenhouse gas Emissions.

862 References

863 Adhikari, K., Hartemink, A. E., Minasny, B., Bou Kheir, R., Greve, M. B., and Greve, M. H.: Digital
864 mapping of soil organic carbon contents and stocks in Denmark, PLoS One, 9,
865 <https://doi.org/10.1371/journal.pone.0105519>, 2014.

866 Ala-aho, P., Soulsby, C., Wang, H., and Tetzlaff, D.: Integrated surface-subsurface model to investigate
867 the role of groundwater in headwater catchment runoff generation: A minimalist approach to
868 parameterisation, *J Hydrol (Amst)*, 547, 664–677, <https://doi.org/10.1016/j.jhydrol.2017.02.023>, 2017.

869 Arents, E. J. M. M., van der Kolk, J. W. H., Hengeveld, G. M., Lesschen, J. P., Kramer, H., Kuikman, P. J.,
870 and Schelhaas, M. J.: Greenhouse gas reporting for the LULUCF sector in the Netherlands -
871 Methodological background, updata 2018, Wageningen, WOt-technical report 113., 2018.

872 Asadzadeh, M. and Tolson, B.: Pareto archived dynamically dimensioned search with hypervolume-
873 based selection for multi-objective optimization, *Eng. Optim.*, 45, 1489–1509,
874 <https://doi.org/https://doi.org/10.1080/0305215X.2012.748046>, 2013.

875 Bechtold, M., Tiemeyer, B., Laggner, A., Leppelt, T., Frahm, E., and Belting, S.: Large-scale
876 regionalization of water table depth in peatlands optimized for greenhouse gas emission upscaling,
877 *Hydrol Earth Syst Sci*, 18, 3319–3339, <https://doi.org/10.5194/hess-18-3319-2014>, 2014.

878 Bechtold, M., Lannoy, G. J. M. De, Koster, R. D., Reichle, R. H., Mahanama, S. P., Bleuten, W.,
879 Bourgault, M. A., Brümmer, C., Burdun, I., Desai, A. R., Devito, K., Grünwald, T., Grygoruk, M.,
880 Humphreys, E. R., Klatt, J., Kurbatova, J., Lohila, A., Munir, T. M., Nilsson, M. B., Price, J. S., Röhl, M.,
881 Schneider, A., and Tiemeyer, B.: PEAT-CLSM: A Specific Treatment of Peatland Hydrology in the NASA
882 Catchment Land Surface Model, *J Adv Model Earth Syst*, 2130–2162,
883 <https://doi.org/10.1029/2018MS001574>, 2019.

884 Bona, K. A., Shaw, C., Thompson, D. K., Hararuk, O., Webster, K., Zhang, G., Voicu, M., and Kurz, W. A.:
885 The Canadian model for peatlands (CaMP): A peatland carbon model for national greenhouse gas
886 reporting, *Ecol Model*, 431, 109164, <https://doi.org/10.1016/j.ecolmodel.2020.109164>, 2020.

887 Børgesen, C. D., Waagepetersen, J., Iversen, T. M., Grant, R., Jacobsen, B., and Elmhold, S.:
888 Midtvejsevaluering af vandmiljøplan III - Hoved- og baggrundsnotater, 2009.

889 DHI: MIKE HYDRO - River - User Guide, Hørsholm, Denmark, 2019.

890 DHI: MIKE SHE - User Guide and Reference Manual, Hørsholm, Denmark, 2022.

891 Duranel, A., Thompson, J. R., Birmingham, H., Durepaire, P., Garambois, S., Wyns, R., and Cubizolle, H.:
892 Modelling the hydrological interactions between a fissured granite aquifer and a valley mire in the
893 Massif Central, France, *Hydrol Earth Syst Sci*, 25, 291–319, 2021.

894 Evans, C. D., Peacock, M., Baird, A. J., Artz, R. R. E., Burden, A., Callaghan, N., Chapman, P. J., Cooper,
895 H. M., Coyle, M., Craig, E., Cumming, A., Dixon, S., Gauci, V., Grayson, R. P., Helfter, C., Heppell, C. M.,
896 Holden, J., Jones, D. L., Kaduk, J., Levy, P., Matthews, R., McNamara, N. P., Misselbrook, T., Oakley, S.,
897 Page, S. E., Rayment, M., Ridley, L. M., Stanley, K. M., Williamson, J. L., Worrall, F., and Morrison, R.:
898 Overriding water table control on managed peatland greenhouse gas emissions, *Nature*, 593, 548–552,
899 <https://doi.org/10.1038/s41586-021-03523-1>, 2021.

900 Friedrich, S., Gerner, A., Gabrielle, C., and Disse, M.: Scenario-based groundwater modeling of a raised
901 bog with Mike She, EGU General Assembly 2023, Vienna, Austria, 24–28 Apr 2023, EGU23-15608,
902 <https://doi.org/https://doi.org/10.5194/egusphere-egu23-15608>, 2023.

903 Jupiter: <https://www.geus.dk/produkter-ydelser-og-faciliteter/data-og-kort/national-boringsdatabase-jupiter>, last access: 12 April 2025.

905 Graham, D. N. and Butts, M. B.: Flexible Integrated Watershed Modeling with MIKE SHE, in: Watershed
906 Models, edited by: Singh, V. P. and Frevert, D. K., CRC Press, 245–272,
907 <https://doi.org/10.1201/9781420037432.ch10>, 2005.

908 Günther, A., Barthelmes, A., Huth, V., Joosten, H., Jurasinski, G., Koebsch, F., and Couwenberg, J.:
909 Prompt rewetting of drained peatlands reduces climate warming despite methane emissions, *Nat*
910 *Commun*, 11, 1–5, <https://doi.org/10.1038/s41467-020-15499-z>, 2020.

911 Gupta, H. V., Kling, H., Yilmaz, K. K., and Martinez, G. F.: Decomposition of the mean squared error and
912 NSE performance criteria : Implications for improving hydrological modelling, *J Hydrol (Amst)*, 377, 80–
913 91, <https://doi.org/10.1016/j.jhydrol.2009.08.003>, 2009.

914 Gyldenkærne, S., Callisen, L. W., Greve, M. H., Beucher, A. M., Weber, P. L., Elsgaard, L., Lærke, P. E.,
915 Stisen, S., Koch, J., and Levin, G.: Opgørelse af CO₂-emissioner fra organiske jorde, Aarhus Universitet,
916 DCE – Nationalt Center for Miljø og Energi, Fagligt notat nr. 2025|01, 29pp pp., 2025.

917 Haahti, K., Warsta, L., Kokkoneen, T., Younis, B. B., and Koivusalo, H.: Distributed hydrological modeling
918 with channel network flow of a forestry drained peatland site, *Water Resour Res*, 246–263,
919 <https://doi.org/10.1002/2015WR018038>.Received, 2015.

920 Henriksen, H. J., Kragh, S. J., Gotfredsen, J., Ondracek, M., M, van, T., Jakobsen, A., Schneider, R., Koch,
921 J., Troldborg, L., Rasmussen, P., Pasten-Zapata, E., and Stisen, S.: Dokumentationsrapport vedr.
922 modelleverancer til Hydrologisk Informations- og Prognosesystem, 2020a.

923 Henriksen, H. J., Kragh, S. J., Gotfredsen, J., Ondracek, M., M, van, T., Jakobsen, A., Schneider, R., Koch,
924 J., Troldborg, L., Rasmussen, P., Pasten-Zapata, E., and Stisen, S.: Dokumentationsrapport vedr.
925 modelleverancer til Hydrologisk Informations- og Prognosesystem, 2020b.

926 Henriksen, H. J., Schneider, R., Koch, J., Ondracek, M., Troldborg, L., Seidenfaden, I. K., Kragh, S. J.,
927 Bøgh, E., and Stisen, S.: A New Digital Twin for Climate Change Adaptation, Water Management, and
928 Disaster Risk Reduction (HIP Digital Twin), *Water (Switzerland)*, 15,
929 <https://doi.org/10.3390/w15010025>, 2023.

930 IPCC: 2013 Supplement to the 2006 IPCC Guidelines for National Greenhouse Gas Inventories :
931 Wetlands, edited by: Hiraishi, T., Krug, T., Tanabe, K., Srivastava, N., Baasansuren, J., Fukuda,
932 M.Troxler, T. G., Published: IPCC, Switzerland, Switzerland, 2014.

933 Jacob, D., Petersen, J., Eggert, B., Alias, A., Christensen, O. B., Bouwer, L. M., Braun, A., Colette, A.,
934 Déqué, M., Georgievski, G., Georgopoulou, E., Gobiet, A., Menut, L., Nikulin, G., Haensler, A.,
935 Hempelmann, N., Jones, C., Keuler, K., Kovats, S., Kröner, N., Kotlarski, S., Kriegsmann, A., Martin, E.,
936 van Meijgaard, E., Moseley, C., Pfeifer, S., Preuschmann, S., Radermacher, C., Radtke, K., Rechid, D.,
937 Rounsevell, M., Samuelsson, P., Somot, S., Soussana, J. F., Teichmann, C., Valentini, R., Vautard, R.,
938 Weber, B., and Yiou, P.: EURO-CORDEX: New high-resolution climate change projections for European
939 impact research, *Reg Environ Change*, 14, 563–578, <https://doi.org/10.1007/s10113-013-0499-2>, 2014.

940 Java, O., Kohv, M., and Lõhmus, A.: Performance of a bog hydrological system dynamics simulation
941 model in an ecological restoration context: Soomaa case study, *Water (Switzerland)*, 13,
942 <https://doi.org/10.3390/w13162217>, 2021.

943 Jutebring, E., Johansson, E., Sjöberg, Y., Huseby, R., and Laudon, H.: Groundwater-surface water
944 interactions across scales in a boreal landscape investigated using a numerical modelling approach, *J*
945 *Hydrol (Amst)*, 560, 184–201, <https://doi.org/10.1016/j.jhydrol.2018.03.011>, 2018.

946 Kirpotin, S. N., Antoshkina, O. A., Berezin, A. E., Elshehawi, S., Feurdean, A., Lapshina, E. D., Pokrovsky,
947 O. S., Peregón, A. M., Semenova, N. M., Tanneberger, F., Volkov, I. V., and Volkova, I. I.: Great Vasyugan
948 Mire: How the world 's largest peatland helps addressing the world 's largest problems, *Ambio*, 50,
949 2038–2049, <https://doi.org/10.1007/s13280-021-01520-2>, 2021.

950 Koch, J., Elsgaard, L., Greve, M. H., Gyldenkærne, S., Hermansen, C., Levin, G., Wu, S., and Stisen, S.:
951 Water-table-driven greenhouse gas emission estimates guide peatland restoration at national scale,
952 *Biogeosciences*, 20, 2387–2403, <https://doi.org/10.5194/bg-20-2387-2023>, 2023.

953 Largeron, C., Krinner, G., Ciais, P., and Brutel-Vuilmet, C.: Implementing northern peatlands in a global
954 land surface model: Description and evaluation in the ORCHIDEE high-latitude version model (ORC-HL-
955 PEAT), *Geosci Model Dev*, 11, 3279–3297, <https://doi.org/10.5194/gmd-11-3279-2018>, 2018.

956 Leifeld, J., Wüst-Galley, C., and Page, S.: Intact and managed peatland soils as a source and sink of
957 GHGs from 1850 to 2100, *Nat Clim Chang*, 9, 945–947, <https://doi.org/10.1038/s41558-019-0615-5>,
958 2019.

959 Lewis, C., Albertson, J., Zi, T., Xu, X., and Kiely, G.: How does afforestation affect the hydrology of a
960 blanket peatland? A modelling study, *Hydrol Process*, 3588, 3577–3588,
961 <https://doi.org/10.1002/hyp.9486>, 2013.

962 Lloyd J., Taylor, J. A.: On the Temperature Dependence of Soil Respiration, *Funct Ecol*, 8, 315–323,
963 1994.

964 Matott, L. S.: OSTRICH – An Optimization Software Toolkit for Research Involving Computational
965 Heuristics Documentation and User 's Guide, Version 17.12.19, New York, 2019.

966 Mozafari, B., Bruen, M., Donohue, S., Renou-wilson, F., and Loughlin, F. O.: Peatland dynamics: A
967 review of process-based models and approaches *Science of the Total Environment Peatland dynamics* :
968 A review of process-based models and approaches, *Science of the Total Environment*, 877,
969 <https://doi.org/10.1016/j.scitotenv.2023.162890>, 2023.

970 Naturstyrelsen: Lavbundsprojekt Ringfenner, Detail- og Myndighedsprojekt, 2022.

971 Nielsen, A. S., Larsen, K. S., Lærke, P. L., Rodriguez, A. F., Pullens, J. W. M., Petersen, R. J., and
972 Christiansen, J. R.: A full year of continuous net soil and ditch CO₂, CH₄, N₂O fluxes, soil hydrology and
973 meteorology for a drained fen in Denmark, *Earth System Science Data Discuss. [preprint]*,
974 <https://doi.org/10.5194/essd-2025-123>, 2025a.

975 Nielsen, O.-K., Plejdrup, M. S., Winther, M., Nielsen, M., Gyldenkærne, S., Mikkelsen, M. H.,
976 Albrektsen, R., Hjelgaard, K., Fauser, P., Bruun, H. G., Levin, G., Callisen, L. W., Andersen, T. A.,
977 Johannsen, V. K., Nord-Larsen, T., Vesterdal, L., Stupak, I., Scott-Bentsen, N., Rasmussen, E., Petersen,
978 S. B., Baunbæk, L., and Hansen, M. G.: Denmark's National Inventory Document 2025. Emission
979 Inventories 1990-2023, 2025b.

980 Oikawa, P. Y., Jenerette, G. D., Knox, S. H., Sturtevant, C., Verfaillie, J., Dronova, I., Poindexter, C. M.,
981 Eichelmann, E., and Baldocchi, D. D.: Evaluation of a hierarchy of models reveals importance of
982 substrate limitation for predicting carbon dioxide and methane exchange in restored wetlands, *J*
983 *Geophys Res Biogeosci*, 122, 145–167, <https://doi.org/10.1002/2016JG003438>, 2017.

984 Olefeldt, D., Euskirchen, E. S., Harden, J., Kane, E., McGuire, A. D., Waldrop, mark P., and Turetsky, M.
985 R.: A decade of boreal rich fen greenhouse gas fluxes in response to natural and experimental water
986 table variability, *Glob Chang Biol*, 23, 2428–2440, <https://doi.org/10.1111/gcb.13612>, 2017.

987 Pasten-Zapata, E., Sonnenborg, T. O., and Refsgaard, J. C.: Climate change: Sources of uncertainty in
988 precipitation and temperature projections for Denmark, Geological Survey of Denmark and Greenland
989 Bulletin, 43, 1–6, <https://doi.org/10.34194/GEUSB-201943-01-02>, 2019.

990 Regeringen: Aftale om et Grønt Danmark - Aftale mellem regeringen, Landbrug & Fødevarer,
991 Danmarks Naturfredningsforening, Fødevareforbundet NNF, Dansk Metal, Dansk Industri og
992 Kommunernes Landsforening - 24. juni 2024, 2024.

993 Regulation (EU) 2024/1991: of the European Parliament and of the Council of 24 June 2024 on nature
994 restoration and amending Regulation (EU) 2022/869, Official Journal of the European Union, 2024.

995 Rigney, C., Wilson, D., Renou-Wilson, F., Müller, C., Moser, G., and Byrne, K. A.: Greenhouse gas
996 emissions from two rewetted peatlands previously managed for forestry, Mires and Peat, 21, 1–23,
997 <https://doi.org/10.19189/MaP.2017.OMB.314>, 2018.

998 Rodriguez, A. F., Pullens, J. W. M., Christiansen, J. R., Larsen, K. S., and Lærke, P. E.: Modeling of
999 greenhouse gas emissions from paludiculture in rewetting peatlands is improved by high frequency
1000 water table data, EGUsphere [preprint], <https://doi.org/10.5194/egusphere-2024-3030>, 2024.

1001 Scharling, M.: Klimagrid Danmark - Nedbør, lufttemperatur og potentiel fordampning 20X20 & 40x40
1002 km - Metodebeskrivelse, Danish Meteorological Institute, 1999a.

1003 Scharling, M.: Klimagrid Danmark Nedbør 10x10 km (ver. 2) - Metodebeskrivelse, Danish
1004 Meteorological Institute, 1999b.

1005 Schneider, R., Koch, J., Troldborg, L., Henriksen, H. J., and Stisen, S.: Machine learning-based
1006 downscaling of modelled climate change impacts on groundwater table depth, 2022.

1007 Seidenfaden, I. K., Sonnenborg, T. O., Stisen, S., and Kidmose, J.: Quantification of climate change
1008 sensitivity of shallow and deep groundwater in Denmark, J Hydrol Reg Stud, 41, 101100,
1009 <https://doi.org/10.1016/j.ejrh.2022.101100>, 2022.

1010 Shi, X., Thornton, P. E., Ricciuto, D. M., Hanson, P. J., Mao, J., Sebestyen, S. D., Griffiths, N. A., and
1011 Bisht, G.: Representing northern peatland microtopography and hydrology within the Community Land
1012 Model, Biogeosciences, 12, 6463–6477, <https://doi.org/10.5194/bg-12-6463-2015>, 2015.

1013 Stenberg, L., Haahti, K., Hökkä, H., Launiainen, S., and Nieminen, M.: Hydrology of Drained Peatland
1014 Forest: Numerical Experiment on the Role of Tree Stand Heterogeneity and Management, Forests,
1015 MDPI, 1–19, <https://doi.org/10.3390/f9100645>, 2018.

1016 Stisen, S., Sonnenborg, T. O., Troldborg, L., and Refsgaard, J. C.: Evaluation of Climate Input Biases and
1017 Water Balance Issues Using a Coupled Surface – Subsurface Model, Vadose Zone Journal, 10,
1018 <https://doi.org/10.2136/vzj2010.0001>, 2011.

1019 Stisen, S., Ondracek, M., Troldborg, L., Schneider, R. J. M., and van Til, M. J.: National Vandressource
1020 Model - Modelopstilling og kalibrering af DK-model 2019, De nationale geologiske undersøgelser for
1021 Danmark og Grønland (GEUS), Rapport 2019/31, 2019.

1022 Tanneberger, F., Abel, S., Couwenberg, J., Dahms, T., Gaudig, G., Günther, A., Kreyling, J., Peters, J.,
1023 Pongratz, J., and Joosten, H.: Towards net zero CO₂ in 2050: An emission reduction pathway for
1024 organic soils in Germany, Mires and Peat, 27, 1–17,
1025 <https://doi.org/10.19189/MaP.2020.SNPG.StA.1951>, 2021.

1026 Tiemeyer, B., Freibauer, A., Borraz, E. A., Augustin, J., Bechtold, M., Beetz, S., Beyer, C., Ebli, M.,
1027 Eickenscheidt, T., Fiedler, S., Förster, C., Gensior, A., Giebels, M., Glatzel, S., Heinichen, J., Hoffmann,

1028 M., Höper, H., Jurasinski, G., Laggner, A., Leiber-Sauheitl, K., Peichl-Brak, M., and Drösler, M.: A new
1029 methodology for organic soils in national greenhouse gas inventories: Data synthesis, derivation and
1030 application, *Ecol Indic*, 109, 105838, <https://doi.org/10.1016/j.ecolind.2019.105838>, 2020.

1031 Wilson, D., Blain, D., Couwenber, J., Evans, C., Murdiyarso, D., Page, S., Renou-Wilson, F., Rieley, J.,
1032 Strack, M., and Tuittila, E. S.: Greenhouse gas emission factors associated with rewetting of organic
1033 soils, *Mires and Peat*, 17, 1–28, <https://doi.org/10.19189/MaP.2016.OMB.222>, 2016.

1034 Wu, Y. and Blodau, C.: PEATBOG: A biogeochemical model for analyzing coupled carbon and nitrogen
1035 dynamics in northern peatlands, *Geosci Model Dev*, 6, 1173–1207, <https://doi.org/10.5194/gmd-6-1173-2013>, 2013.

1037 Wunsch, A., Liesch, T., and Broda, S.: Deep learning shows declining groundwater levels in Germany
1038 until 2100 due to climate change, *Nat Commun*, 13, 1–13, <https://doi.org/10.1038/s41467-022-28770-2>, 2022.

1040 Yuan, F., Wang, Y., Ricciuto, D. M., Shi, X., Yuan, F., Brehme, T., Bridgman, S., Keller, J., Warren, J. M.,
1041 Griffiths, N. A., Sebestyen, S. D., Hanson, P. J., Thornton, P. E., and Xu, X.: Hydrological feedbacks on
1042 peatland CH₄ emission under warming and elevated CO₂: A modeling study, *J Hydrol (Amst)*, 603,
1043 127137, <https://doi.org/10.1016/j.jhydrol.2021.127137>, 2021.

1044 Zscheischler, J., Martius, O., Westra, S., Bevacqua, E., Raymond, C., Horton, R. M., van den Hurk, B.,
1045 AghaKouchak, A., Jézéquel, A., Mahecha, M. D., Maraun, D., Ramos, A. M., Ridder, N. N., Thiery, W.,
1046 and Vignotto, E.: A typology of compound weather and climate events, *Nat Rev Earth Environ*, 1, 333–
1047 347, <https://doi.org/10.1038/s43017-020-0060-z>, 2020.

1048

1049